Forecast of Low Clouds over a Snow Surface in the Arctic Using the WRF Model

M. HAGMAN,[a] G. SVENSSON,[a] AND W. M. ANGEVINE[b,c]

[a] *Department of Meteorology, Stockholm University, Stockholm, Sweden*
[b] *CIRES, University of Colorado Boulder, Boulder, Colorado*
[c] *NOAA/ESRL/CSD, Boulder, Colorado*

(Manuscript received 6 December 2020, in final form 7 May 2021)

ABSTRACT: The Swedish Armed Forces configuration of the Weather Research and Forecasting (WRF) Model has problems in forecasting low clouds in stably stratified conditions when the ground is covered by snow. Reforecasts for January and February 2018, together with observations from Sodankylä in northern Finland, are analyzed to find the cause. The investigation is done iteratively between the single-column model (SCM), applied at Sodankylä, and the full 3D version. Our experiments show that the forecast error arises due to inadequate initialization of stratocumulus (Sc) clouds in WRF using the ECMWF global model, Integrated Forecasting System (IFS). By including bulk liquid water and bulk ice water content, from IFS in the initial profile, the downwelling longwave radiation increases and prevents the near-surface temperature from dropping abnormally. This, in turn, prevents artificial clouds from forming at the first model level. When no clouds are present in the IFS initial profile, the Sc clouds can be initialized using information from the observed vertical profiles. Generally, initialization of Sc clouds in WRF improves the forecast substantially.

KEYWORDS: Boundary layer; Cloud cover; Cloud parameterizations; Clouds; Model initialization

1. Introduction

a. Background

During the last 10-yr period the Swedish Armed Forces (SAF) has utilized the Advanced Weather Research and Forecasting Model (WRF-ARW; Skamarock et al. 2008), to issue forecasts for Scandinavia and for international operations, e.g., Afghanistan, Mali, and Iraq. During this time, it has been noticed that the model, at times, has severe problems to represent low clouds. The problem is pronounced over the northern parts of Scandinavia, over snow-covered ground, when the boundary layer is stably stratified. In these situations, WRF tends to form low clouds over an area that is too widespread and too long-lived compared to what is observed. It is a typical winter phenomenon and does not exist in warm conditions. Generally, this problem does not seem to appear to the same extent in the Integrated Forecasting System (IFS; Owens and Hewson 2018), HARMONIE-AROME (Bengtsson et al. 2017) or in the High Resolution Limited Area Model (HIRLAM; Undén et al. 2002)-models (for model terms, see Table 1). Although, not as severe problems as in WRF, e.g., IFS shows problems in Arctic conditions (Tjernström et al. 2021). An ensemble forecast system (EPS) comprising 20 members has also been run in SAF, unfortunately, without any improvement of the artificial low clouds. Nevertheless, Price et al. (2015) showed that EPS can be used to improve forecasting of persistent fog. The aim of this study is to reveal what causes this overrepresentation of low clouds in the SAF configuration of WRF, and to propose improvements.

Corresponding author: M. Hagman, hackesailor@hotmail.com

b. Characteristics of the stable boundary layer

Turbulence is weak under stably stratified conditions, so other small-scale processes, such as drainage flow, gravity waves, and fog and dew formation become important (Sun et al. 2015; LeMone et al. 2019). During the last 15 years, as part of the Global Energy and Water Exchanges (GEWEX) Atmospheric Boundary Layer Study (GABLS; Holtslag et al. 2012), much focus has been on model representation of the stably stratified boundary layer (SBL) in models. Both operational and research models participate in the single-column model (SCM) intercomparisons and it is revealed that mixing in the SBL in operational models is generally too large. WRF, in different configurations, has been taking part in two GABLS studies (Svensson et al. 2011; Bosveld et al. 2014). A strong underestimation of the diurnal cycles of the 2 m temperature and the 10 m wind speed was generally found (Svensson et al. 2011) for a location in the middle of United States (CASES-99; Poulos et al. 2002). Although surface temperature was prescribed, 2 m temperature during the first night had a cold bias in many models, including WRF. Contrary to most of the participating models, both WRF Yonsei University (YSU; Hong and Pan 1996) planetary boundary layer (PBL) scheme and WRF Mellor–Yamada–Janjić (MYJ; Hu et al. 2010) TKE scheme showed too-low wind velocities at low levels during nighttime, due to an imposed lower limit on the friction velocity. This, in turn, led to low values of downward sensible heat fluxes in the SBL. The results are more homogenous in the intercomparison experiment where the boundary layer is coupled to a land surface model (Bosveld et al. 2014) as interactions with the land surface are very important, especially for the SBL (Holtslag et al. 2013).

c. SBL over snow

SBLs are a real challenge for Numerical Weather Prediction (NWP) models (Holtslag et al. 2013) as discussed above. This is

DOI: 10.1175/MWR-D-20-0396.1

TABLE 1. List of model term abbreviations.

WRF	Weather Research and Forecasting Model
ARW-WRF	Advanced Research WRF
SAF	Swedish Armed Forces
SAF WRF	SAFs configuration of WRF
SCM	Single-column model
WRF SCM	WRF single-column model
WRF 3D	WRF full 3D model
ECMWF	European Centre for Medium-Range Weather Forecasts
IFS	Integrated Forecast System
IFS HRES	Atmospheric Model High Resolution of the IFS (ECMWF global model)
HARMONIE	HIRLAM-ALADIN Research on Mesoscale Operational NWP in Euromed
AROME	Applications of Research to Operations at Mesoscale
HARMONIE-AROME	Reference model configuration of AROME
GEWEX	Global Energy and Water Exchanges
GABLS	Atmospheric Boundary Layer Study of GEWEX

especially the case when the ground is snow-covered in polar regions as the conditions can become very stable (Sterk et al. 2015). One of the characteristics of snow is that it acts almost as a blackbody over the thermal infrared part of the spectrum; emissivities range between 0.96 and 0.99 (Zhang 2005). The outgoing longwave radiation increases according to Stefan–Boltzmann's law, thus efficiently cooling the snow surface. Snow also has an extremely low thermal conductivity, especially new fresh dry snow with low density, and therefore acts as a very good insulator between the air above and the ground below. On nights without clouds, the snow surface can thus cool very strongly by emitting longwave radiation. Add to this the high albedo of the snow, which during days reflects a lot of incoming shortwave radiation, thus lowering the temperature of the snow surface.

The polar regions are covered with snow for many months every year. Without a good representation of the snowpack during the winter season it is problematic to model the temperature gradient in the snow. A multilayer snowpack representation (Arduini et al. 2019) can produce a sharper gradient in the upper parts, compared to a bulk snowpack representation. In Savijärvi (2014) the evolution of the skin temperature and the 2 m temperature is compared between a two-layer force and restore scheme and a five-layer snow scheme. The two-layer scheme does a good job during the day, but has a warm bias during night.

In this study the WRF Model, as it is based on the SAF configuration, is run with the Noah land surface model (Chen and Dudhia 2001), which has a bulk snowpack description with just one temperature at the top of the snowpack, i.e., the skin temperature of the pack itself. To calculate the temperature gradient in the snow this skin temperature, together with the temperature in the middle of the first soil layer, at a depth of 5 cm, is used to calculate the gradient. In reality the snow skin temperature is cooler than the rest of the snowpack during night and warmer during day. This produces a nonlinear structure of the temperature gradient within a snowpack layer, where the temperature drops quickly in the uppermost part of the snowpack (Sultana et al. 2014). This nonlinear structure cannot be represented with the Noah land surface model bulk representation of the snowpack. In the Rapid Update Cycle Land Surface Model (RUC LSM; Smirnova et al. 2016), which is also available in WRF, the snowpack is divided into two layers when snow depth is more than 7.5 cm.

d. Clouds

During wintertime, northern Scandinavia is often under the influence of a ridge of high pressure and prevailing weak or moderate northeasterly winds. Stratocumulus (Sc) clouds are common in these subsidence regimes. Here, the low-level airflow supplies moisture from the open Barents Sea in the north, which can make the clouds quasi-stationary for days with associated light snowfall. These Sc clouds may consist of both ice and liquid water, of which liquid water interacts most effectively with longwave radiation. Typical cloud-top temperatures of these Sc clouds in this study vary between −10° and −20°C. The cloud-top radiative cooling creates sinking air parcels that creates convection in the cloud and may make it well mixed (Stull 1988). The convection generated at cloud top many times affects the whole atmospheric boundary layer (ABL), although surface fluxes are usually small. Other important large-scale dynamics that affect the Sc cloud are subsidence and the thermodynamic conditions above the cloud deck. When Sc is present, it blocks much of the outgoing longwave radiation, and the snow surface does not cool rapidly (LeMone et al. 2019).

During periods of low winds when the sky is clear, the condition is favorable for a surface inversion to form. In a weak wind situation, the downward transport of sensible heat to the surface is much smaller than the outgoing longwave radiation from the snow surface. The energy budget at the surface must balance out to zero, forcing the temperature to decrease in order to balance the ground heat flux. Because the specific humidity in cold Arctic air is very low (mostly less than 1 g water vapor per 1 kg air), and saturation water vapor pressure over ice is lower than over liquid water, fog rarely forms in these conditions. The situation is totally different if the temperature is above zero and snow is melting, then radiation fog quickly forms. Two types of radiation fog may form (e.g., Stull 1988): One type that is most dense close to the ground (stable

fog) and gets more diffuse when height increases, and one type that is well mixed with a well-defined cloud top (adiabatic fog). The latter is more like a Sc cloud.

e. Initialization of clouds in NWP

A number of different attempts have been made to assimilate or initialize clouds into NWP from the very first time step of the forecast run. For example Yucel et al. (2002) used cloud cover from visible band Geostationary Operational Environmental Satellite (GOES) data to improve the Regional Atmospheric Modeling System (RAMS). The observation of radiances and cloud fraction were used to derive the vertical distribution of cloud ice and cloud liquid water in the model. These variables were then used to update the cloud cover in the model. This consistently improved shortwave radiation, longwave radiation, and precipitation fields in the model. Prior cloud ingestion improved the cloud forecasts up to 4 h into the model run. Another study used a nowcasting Satellite Application Facility (Dybbroe et al. 2005) based on Meteosat Second Generation (MSG) product, (Schmetz et al. 2002) to improve initial cloudiness in the High Resolution Limited Area Model (HIRLAM; van der Veen 2013). The reference runs from HIRLAM often had too few clouds initially. In more than 80% of the cases the cloud ingestion led to better cloud-cover forecasts, and in more than 50% it lasted as long as 24 h into the forecast. In 2019 (J. Pyykkö 2019, personal communication) applied a similar method as van der Veen (2013) using cloud information from the Mesoscale Analysis system (MESAN; Häggmark et al. 2000) to change specific humidity, temperature, and hydrometeor concentrations in the HARMONIE-AROME model system. This study showed that the signal from these alterations can last over 12 h. None of these studies, though, focused on initialization of clouds in stably stratified conditions over snow. In the Rapid Refresh assimilation/model system, (RAP; Benjamin et al. 2016), which also uses WRF, a three-dimensional cloud-coverage observation assimilation field is generated. Then, this cloud coverage is used to generate cloud ice and cloud water, which is used to modify background hydrometeor fields in the hourly run assimilation cycle. Also, the Met Office uses variational analysis to assimilate cloud coverage in the Unified Model (Renshaw and Francis 2011). In recent years so-called all-sky satellite data assimilation has been started to be used in IFS, which assimilates all observations directly as radiances, whether they are clear, cloudy, or precipitating (Geer et al. 2018).

In this study we focus on the impact of the initial profiles and the parameterizations that are important in situations when we have low clouds and stably stratified conditions. Specific issues arise in these conditions and our investigations focus on the initialization of clouds and, secondarily, the vertical thermodynamic structure. As in the operational configuration, initial conditions are taken from the Atmospheric Model High Resolution (HRES), of the Integrated Forecast System (IFS; Owens and Hewson 2018) The improvements reported here came from ingesting additional information from the host model on cloud liquid water and cloud ice content into WRF at the beginning of the model run, or from initializing with an observed sounding.

2. WRF Model

The Weather Research and Forecasting (WRF) Model is a numerical weather prediction model designed for research as well as for operational applications (Skamarock et al. 2008). It is highly modular with multiple physics package options. An in-depth description of the numerical model and options on how to configure it can be found in Skamarock et al. (2008). The specific choices of parameterizations in the operational configuration using WRF version 3.9.1.1 for the SAF are summarized in Table 2.

An updated version (Hong et al. 2006) of the original YSU first-order scheme (Hong and Pan 1996) is used in the SAF configuration. The update concerns the critical bulk Richardson number in YSU, which here is as a function of the surface Rossby number. Poor performance of the PBL and/or surface layer schemes could contribute to problems with the forecasts; however, we ran tests with other schemes and found no significant improvement in these cases.

3. Observations

Sodankylä is situated in northern Finland, which is within the domain of SAF Scandinavian forecast area (Fig. 1). The observational site is centered around 67.368°N, 26.633°E and is the heart of Arctic Research Centre of the Finnish Meteorological Institute (FMI ARC) in northern Finland (Kangas et al. 2016). The terrain is moderately undulating, with isolated fells reaching up to 500 m altitude. The observatory is located on the eastern bank of the river Kitinen, 7 km southeast of the Sodankylä town center, and about 100 km north of the Arctic Circle and Rovaniemi. The vegetation mostly consists of coniferous forest and open wetlands. During the period of interest, the ground was frozen and covered by snow with depths between 60 and 80 cm, i.e., the nature of the ground is less important. Sodankylä is one of the supersites with increased observations during the special observation periods of the Year of Polar Prediction, a flagship activity of The Polar Prediction Project (Jung et al. 2016). Here, we are using observations during special observation period 1, February and March 2018, when soundings were launched every 6 h instead of every 12 h.

Observations from the automatic weather station and radiosonde (Vaisala) launches from the sounding station (67.367°N, 26.629°E) are used. The radiation components of the surface energy budget are also observed at this location, while the radiation measurements at the micrometeorological tower (67.362°N, 26.638°E) are mainly auxiliary data to the turbulent fluxes. Backscatter data from a ceilometer (Vaisala CT25K, 905 nm) installed at the Integrated Carbon Observing system (ICOS) tower (67.362°N, 26.639°E) is also used for the period January and February 2018. Liquid and mixed-phased cloud bases are easily detected from the backscatter values. The signal is attenuated by the cloud such that cloud tops can only be observed if the clouds are less than 300 m deep.

4. Model experiments

This study is based on WRF version 3.9.1.1 together with WRF Preprocessing System (WPS) version 3.9.1. The horizontal

TABLE 2. Physics packages in SAF configuration of WRF3.9.1.1, reference cases.

Type of scheme	Scheme
Surface layer	Revised MM5 Monin–Obukhov scheme (Jiménez et al. 2011)
Planetary boundary layer (PBL)	Yonsei University (YSU; Hong 2010)
Land surface model	Unified Noah land surface model (Chen and Dudhia 2001)
Microphysics	Thompson scheme (Han et al. 2013)
Radiation	Rapid Radiative Transfer Model for Global Circulation Models GCM (RRTM-G; Mlawer et al. 1997)

grid spacing is 3 km and the domain over Scandinavia consists of 701 grid points from north to south and 428 grid points from west to east (Fig. 1). The operational version uses 90 vertical levels, with the lowest mass (pressure) level about 9 m above ground. The model is initialized with fields from IFS, with 137 levels. The model top in SAF configuration is around 24 km and 90 IFS levels are overlapped. WRF levels are denser below 10 km and IFS levels are denser above 10 km. Boundary values also come from IFS. Because of operational constraints, every second horizontal grid point from IFS HRES are used (18 km spacing). Operationally, a new forecast is started every 6 h. For instance, a 0000 UTC, run is based on a cold start at 1800 UTC, which is run for 6 h to get the first guess. This first guess is then altered by observations using three-dimensional variational data assimilation, 3D-Var, (Courtier 1998) to produce the analysis for the 0000 UTC run. In this study, however, we do not let the model spin up for 6 h and no data assimilation is carried out. The model is cold-started for every simulation. The model is run with a time step of 20 s and radiation is called every 30th time step (10 min).

The horizontal grid spacing was held constant at 3 km in all experiments and 90 vertical levels were used. The initial model evaluation to establish the signature of the low-level cloud model error is of the operational version, which at that time used 46 vertical levels. The parameterizations used in the operational version of WRF in the SAF (see Table 2) are used as the starting point for the experimentation. Soil temperature and soil moisture are initialized in the same way as other variables, directly from IFS HRES, so there is no spin up for the soil parameters. On the other hand, as mentioned above, the ground is frozen and covered by snow, which makes the spinup less important. IFS HRES uses The Tiled ECMWF Scheme for Surface Exchanges over Land (HTESSEL; Balsamo et al. 2009), which, just like Noah LSM, has 4 soil levels. Even the skin temperature of the snow and the snow depth are initialized from IFS HRES.

The weather during January and February 2018 in northern Scandinavia was often influenced by high pressure that over snow-covered areas typically supports low-level clouds. In these situations, the operational forecast exhibited excess ground-based cloudiness. The low-level (500–2000 m) but not ground-based clouds were often missing, replaced by a ground-based cloud (fog) layer. A selection of dates are rerun and compared with observations from Sodankylä to investigate the model behavior (see Table 3).

To eliminate parameterization, horizontal and vertical interpolation and, finally, vertical resolution as the main reason for the excess cloudiness, we changed these one at a time to see if the model still exhibited excess low-level, ground-based cloudiness (results not shown). As these initial tests revealed that the initialization of the model indeed caused problems, several options on how to best alleviate that were tested. To isolate local physical processes from the large-scale dynamics, and to be able to do numerous tests faster, a single-column model (SCM; Hacker and Angevine 2013; Angevine et al. 2018) of the same WRF version was configured. First a way to initialize clouds into the SCM was devised, and then this method was generalized in the 3D version.

Cloud information (cloud bulk liquid water and ice from IFS HRES) are initialized from the very first time step, in three different ways, to get the forecast to better conform with observations. In method A, clouds were introduced to the model by interpolation of cloud liquid water and cloud ice from IFS HRES analysis. Here, the profile (temperature, water vapor mixing ratio) is not changed to achieve saturation. In method B,

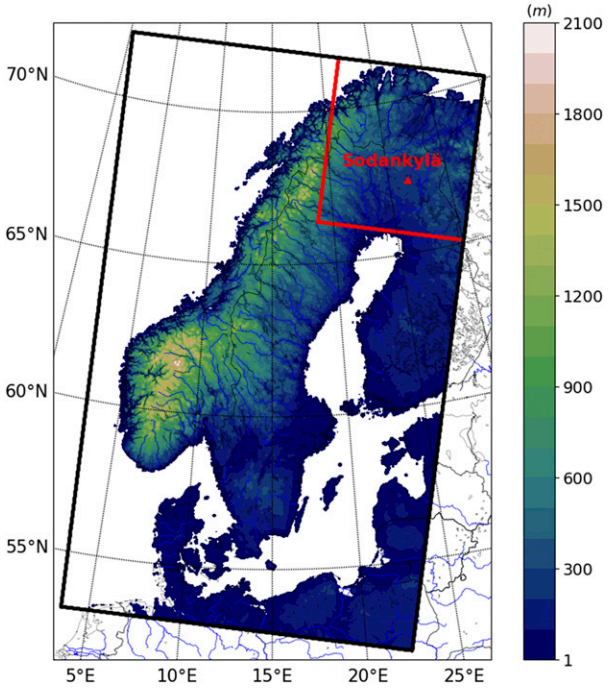

FIG. 1. WRF domain in SAF configuration covering Scandinavia and Finland. Terrain height is in meters (m).The observational site Sodankylä is marked with a red triangle and the area where the initialization is applied in the subsection titled "Case study 1: 18 February 2018" in section 5 is outlined with two red lines.

TABLE 3. Experimental configuration for initialization cases.

Dates	Synoptic situation and cloud liquid water in IFS HRES	Initialization type	Parameterization
18 Feb 2018	Ridge of high pressure stretches from south to north over Scandinavia; T850: −10° to −15°C; Sc in observations, slowly dissipating	SCM: Cloud liquid water (QC) from IFS Interpolation from IFS (method A)	Reference SAF configuration (see Table 1)
	Altitudes of cloud liquid water in IFS HRES almost coinciding with observations and possible to initialize into WRF	Interpolation and T to Td in clouds (method B) Threshold QC $> 1 \times 10^{-2}$ g kg^{-1} at model levels Interpolation and water vapor mixing ratio (Wv) to saturation water vapor mixing ratio (Wv max) in clouds (method C) Threshold QC $> 1 \times 10^{-2}$ g kg^{-1} at model level. 3D: As in SCM, but cloud ice (QI) also transferred	
20 Feb 2018	Ridge of high pressure stretches from north to south over Scandinavia; patches of Sc over the Northern region; otherwise, mostly clear skies over northern Sweden and big parts of Finland, T850: −15° to −20°C; weak alternating winds; 2 m temperature: −15 to −30°C	As in 18 Feb 2018	Reference SAF configuration (see Table 1)
	No cloud liquid cloud water in IFS HRES to transfer	No liquid cloud liquid water to initialize from IFS HRES at Sodankylä	
26 Feb 2018	Strong high pressure is situated over the Arctic Ocean and a ridge of high pressure stretching down over Scandinavia; Sc over Finland moves westward over northern parts of Sweden; T850: −10° to −15°C; northeasterly winds	As in 18 Feb 2018	Reference SAF configuration (see Table 1)
	Too small amount of cloud liquid water in IFS to transfer	Too small amount of or no cloud liquid water to initialize from IFS HRES at Sodankylä θ_l initialization from Sodankylä sounding and Wv to Wv max (method D) (not shown)	
27 Feb 2018	Ridge of high pressure tilting toward southwest; T850: −15° to −20°C; Sc dissipating and moving westward; northeasterly winds	As in 18 Feb 2018	Reference SAF configuration (see Table 1) and PBL TKE scheme MYNN (Nakanishi and Niino 2009) in SCM and 3D
	No cloud liquid water in IFS HRES to transfer	No liquid cloud liquid water to initialize from IFS HRES at Sodankylä θ_l initialization from Sodankylä sounding and Wv to Wv max (method D) θ_l initialization of cloud liquid water and temperature profile below 350 m from Sodankylä sounding at every grid point and Wv to Wv max (method D)	

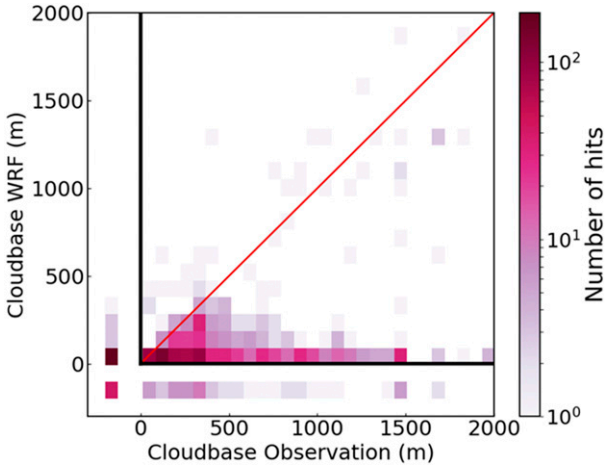

FIG. 2. Two-dimensional histogram of cloud-base observations (m) from AWS at Sodankylä and reference (operational) model results from the corresponding grid box for hourly data for 24 h consecutive simulations during the periods 0000 UTC 1 Jan and 2300 UTC 28 Feb 2018. The model cloud base is defined as the first vertical level where cloud fraction exceeds 80%.

temperature was lowered to the dewpoint at all model levels where the introduced cloud liquid water exceeded a certain value. In method C, water vapor mixing ratio was increased to the saturation water vapor mixing ratio at all altitudes with introduced liquid water content above a threshold. Finally, in method D, clouds were initialized at levels where clouds existed in the Sodankylä sounding. At these levels water vapor mixing ratio was increased to saturation water vapor mixing ratio to better support the clouds.

Four dates when observations from Sodankylä showed Sc clouds at 0000 UTC were chosen (see Table 3). In three of these cases, where IFS HRES deviates from observations, the initialization of clouds was altered through a procedure that considers cloud information from soundings explicitly (method D), and not just implicitly via the IFS HRES analysis that is initialized into WRF.

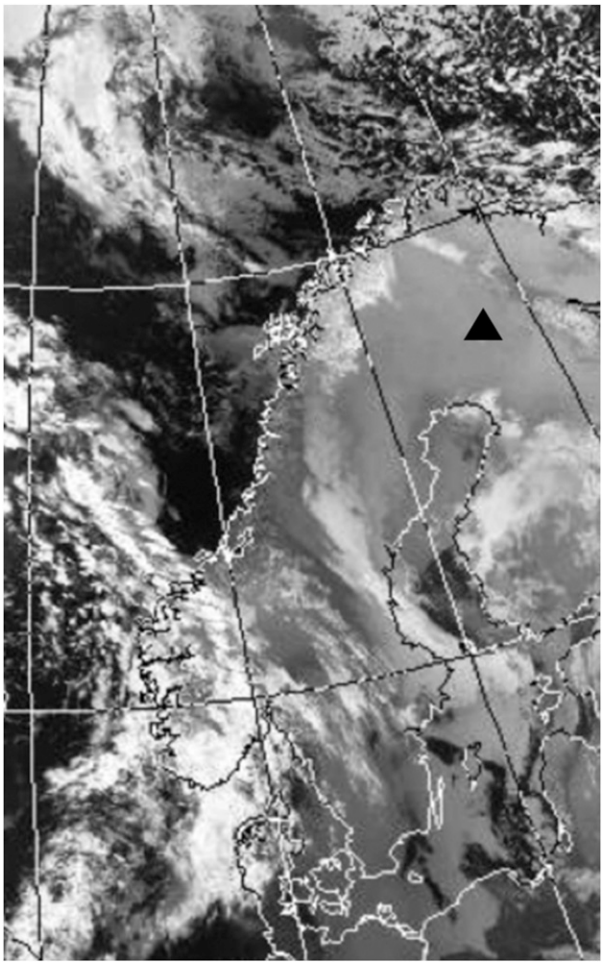

FIG. 3. Satellite IR image at 0323 UTC 18 Feb 2018 from the Advanced Very High Resolution Radiometer (AVHRR), channel 5 (10.5–12.5 μm), showing extensive areas of Sc clouds (dark gray) over the northern parts of Scandinavia. Over the northwestern parts of the Scandinavian mountain range, skies are clear and the light gray (colder) surface appears. Sodankylä is marked with a black triangle. Image is courtesy of NERC Satellite Receiving Station, Dundee University, Scotland, 2020 (http://www.sat.dundee.ac.uk/).

5. Results

The cloud base (below 2000 m) in the SAF operational version of WRF for consecutive 24 h forecasts for January and February (Fig. 2) is evaluated with the automatic weather station data. The model cloud base is here the lowest model level where the cloud fraction exceeds 80%. The value of 80% was set on the fly, when SAF started to run WRF. Practically this value could be set to 50% instead (as it is in IFS HRES parameter ''ceiling''), because the Xu and Randall cloud fraction parameterization (Lazarus and Krueger 1999) almost always gives values of 0% or 100%. In the observations the lowest level where clouds are observed is set to the cloud-base height. One can argue about this, but it strengthens the result of this study, e.g., when the observed lowest layer consists of a small amount, and the cloud-base height in reality is even higher. Also, small amounts of Sc clouds are quite rare during the Arctic winter. Anyway, it is very clear that the model exhibits excess very low-level cloudiness with too-low cloud bases (most commonly fog in the model). The values below and to the left of the bold black straight lines show when the model and the observations have clear skies, respectively. For example, the darkest red square represents cases where it is clear in reality, but the model has clouds at a very low altitude. One can question if cloud-base height, based on cloud fraction amounts at different vertical levels, is a good way to compare model output with observations. This question is further discussed below.

The vertical interpolation can cause problems in the initial state, especially if there are substantial differences in the vertical resolution and if the regional model has coarser resolution than the host model, as in the operational configuration

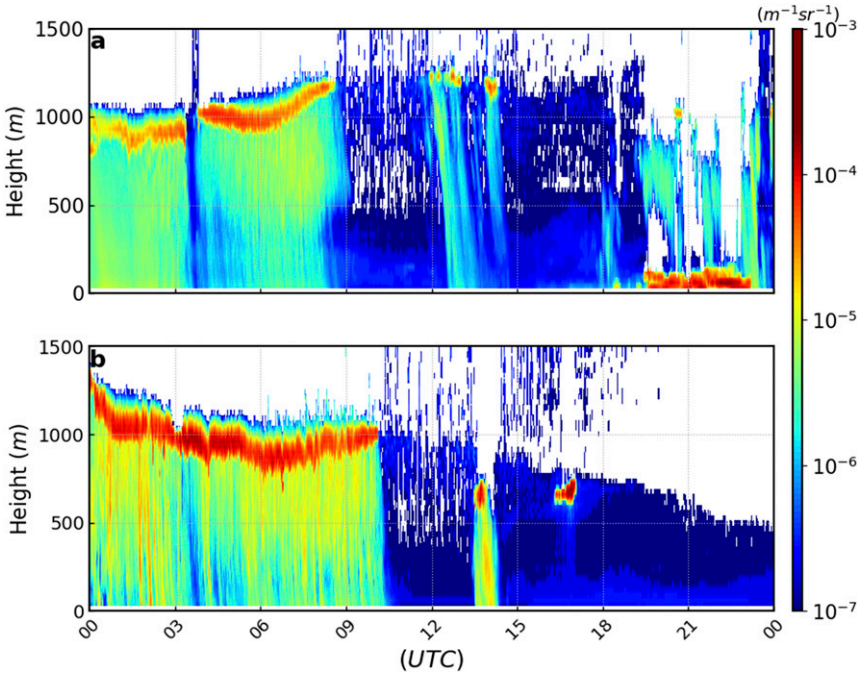

FIG. 4. Backscatter coefficient ($m^{-1}\,sr^{-1}$) from a ceilometer installed at the Integrated Carbon Observing system (ICOS) tower (67.362°N, 26,639°E): (a) 0000 UTC 18 Feb–0000 UTC 19 Feb 2018 and (b) 0000 UTC 27 Feb–0000 UTC 28 Feb 2018.

considered here. Liquid water in a thin layer can be diluted in the interpolation so that the resulting layer is unsaturated. Furthermore, in very cold Arctic airmasses that have low moisture content, it is very important that the vertical interpolation of humidity is done in RH and not in specific humidity. According to the saturation water vapor pressure–temperature dependence at low temperatures, very small amounts of water vapor, that is moved vertically in an interpolation process, can give rise to big changes in RH and erroneously form clouds, especially in the case of sharp inversions and coarse vertical interpolation, e.g., at the surface or in Sc-topped boundary layers. This is not a problem in WRF as RH is used (Skamarock et al. 2008).

Initialization of low-level clouds

To find the cause of the deficiencies in the cloud forecast, two case studies are chosen, 18 and 27 February 2018 (Table 3). For each case, short simulations in the SCM framework for the Sodankylä location are performed and compared with observations. These simulations are done without large-scale forcing, i.e., horizontal and vertical advection. Some concluding insights are then tested in 3D simulations that allow evaluation on a larger scale.

1) CASE STUDY 1: 18 FEBRUARY 2018

The satellite picture on 18 February shows a low cloud deck over the area of interest (Fig. 3), which is confirmed in the observations at Sodankylä where a thin (about 200 m thick) cloud with base at 700–800 m and top around 1000 m is observed between 0000 and 0900 UTC (Fig. 4a). The forecast (Fig. 5a) shows the typical bad behavior with widespread fog. Four different SCM simulations were performed for the site of Sodankylä with start from the 3D initialized profile at 0000 UTC. The reference simulation without initialization of cloud liquid water or cloud ice (as in the original operational configuration) and by adding cloud liquid water and modifying the vapor mixing ratio and temperature according to methods A, B, and C, respectively. In the SCM runs, the cloud liquid water, not ice, is initialized because of the stronger influence on the longwave radiation and thereby the surface energy budget. At the temperature regimes observed at this location and time of year, clouds frequently consist of both liquid water and ice.

Figure 6 shows the results from four different SCM simulations. Without initialization of cloud liquid water content (Fig. 6a), it takes some time for the cloud to form and it does so in the lowest model level and as time goes by it slowly spreads vertically. The reason for this is that in the absence of clouds when the model starts, the downwelling longwave radiation to the surface is relatively small and at the same time the outgoing longwave radiation is relatively large. The skin temperature of the snow surface drops unphysically at the very first model steps (in about 40 s as the model time step is 20 s) from about −12° to near −30°C (blue line in Fig. 6e); a drop of almost 20°C. This is far from what is observed in reality in cloud free situations. It turns out that the model parameterization (in this case how the components of the surface energy budget equation are parameterized) calling sequence matters. The skin temperature is solved for in an iteration process in the Noah land surface model (Sultana et al. 2014) and the radiation

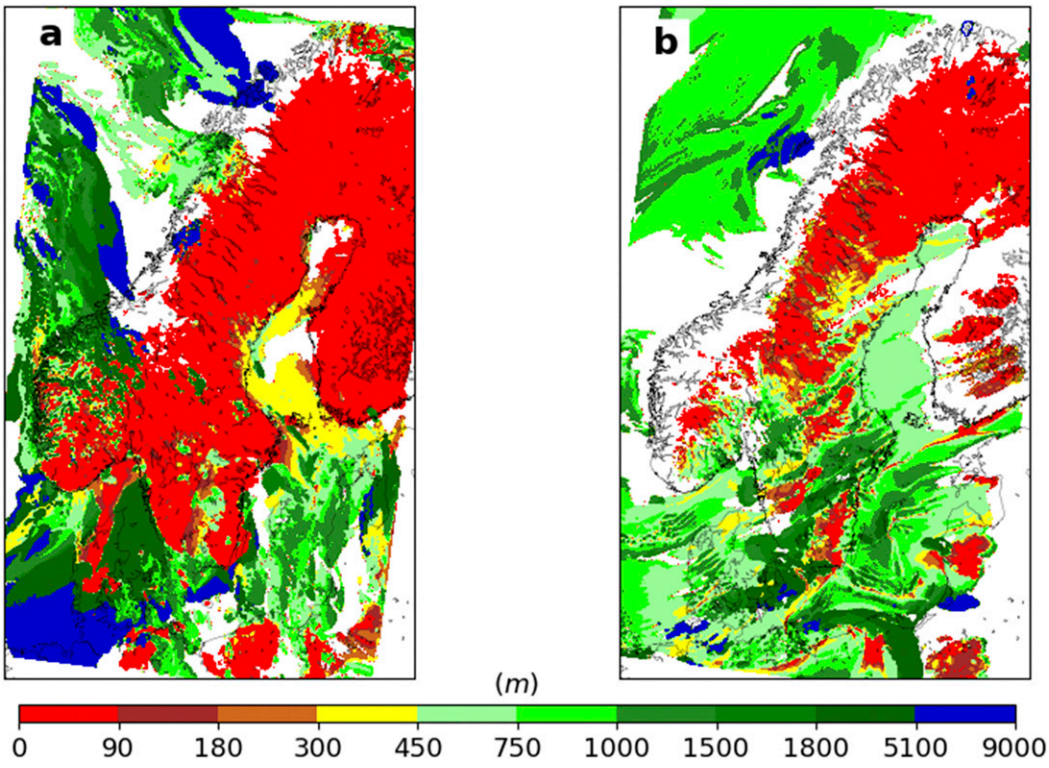

FIG. 5. Cloud-base height (m) for (a) a 6 h simulation started at 0000 UTC 18 Feb 2018 and (b) a 6 h simulation started at 0000 UTC 27 Feb 2018 for SAF reference configuration using YSU PBL parameterization and Xu and Randall cloud fraction parameterization scheme.

module is called for every 30th time step, which leads to a constant skin temperature for the first 10 min (Fig. 6e). When the clouds form at the first model level, the temperature of the cloud top drops because of emission of longwave radiation. This is seen in the dense packing of potential temperature isolines at the cloud top (Fig. 6a). The model supports the clouds and they can slowly grow vertically in this subsidence free environment; however, the evolution is far from realistic. In reality, liquid water cloud at the top of a cold snow surface is not stable in time. The saturation water vapor pressure over snow is lower compared to what it is over liquid water, i.e., cloud droplets. This makes the cloud liquid water deposit on the snow surface.

At about 1000 m altitude, the gradient of the potential temperature is larger (Fig. 6a). This is a sign that Sc clouds existed at these levels in the profile inherited from the IFS HRES, but the cloud liquid and ice are not transferred in the initialization, and WRF cannot form these clouds. Instead it enters into a regime with freezing fog at the lowest model levels without any Sc clouds at all.

Figure 6b shows results from a SCM simulation where cloud liquid water from IFS HRES is used in the initial profile (method A). The values are simply interpolated from the vertical levels in IFS HRES to the WRF vertical grid. By this correction of the initial profile, WRF is now able to form Sc clouds slightly above 1000 m altitude. This increases the longwave radiation from the cloud to the snow surface, which prevents the skin temperature to drop more than 1°–2°C (yellow line in Fig. 6e). The cloud top of the Sc clouds is cooled, which starts upside-down convection from the cloud top down into the cloud and below. The clouds are getting more well mixed and the vertical gradient of the potential temperature decreases (Fig. 6b). Because the cooling at the surface is reduced, compared to the reference run, the near-surface air temperature remains above saturation and no clouds form close to the surface. In reality the cloud base is between 900 and 1000 m, slowly rising until 0900 UTC, when it dissipates completely (Fig. 4a). This evolution is not captured in the SCM, which may be due to the lack of large-scale advection and subsidence. Probably, the clouds in reality dissipate because of the subsidence in the high pressure ridge.

In Fig. 6c, the mixing ratio at vertical levels with cloud liquid water amount greater than $1 \times 10^{-2}\,\mathrm{g\,kg^{-1}}$ in the IFS is set to saturation water vapor pressure in addition to the initialized cloud liquid water (method C). Cloud liquid water now forms from the very first time step, but the amounts are too large, making the skin temperature rise too much compared to observations.

Finally, instead of initializing cloud liquid water and raising water vapor mixing ratio, liquid water is initialized and temperature is lowered to the dewpoint (method B), at the same altitudes, which also makes the initial RH = 100% in the initial profile. This creates a static instability in the temperature profile, which is remixed at the start of the simulation (Fig. 6d).

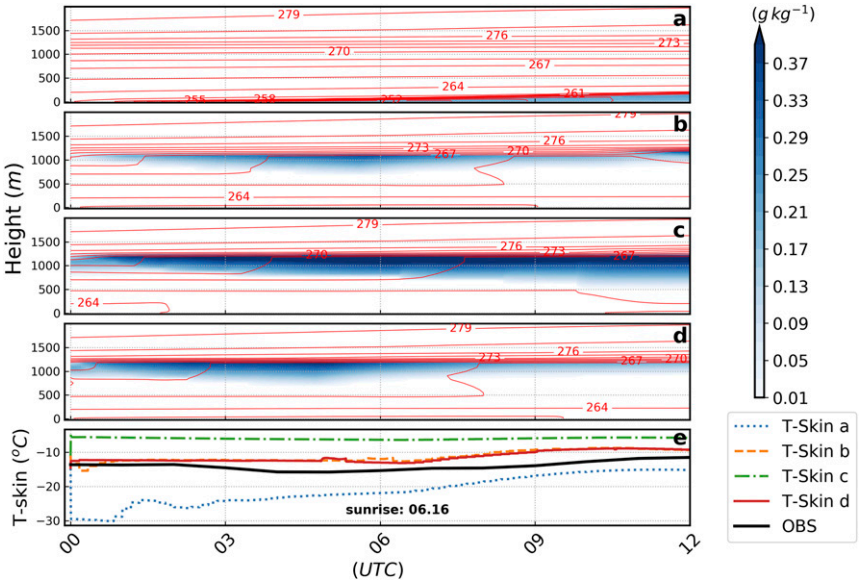

FIG. 6. Height–time cloud liquid water (g kg^{-1}) and potential temperature (K) for 12 h SCM simulations started at 0000 UTC 18 Feb 2018. (a) Reference case, (b) initialization with method A, (c) initialization with method C, (d) initialization by method B, and (e) skin-temperature evolution for simulations in (a)–(d) and retrievals based on downwelling longwave radiation at the surface at the micrometeorological tower (67.362°N, 26.638°E).

This procedure creates dense clouds at the beginning of the run and a realistic development of the skin temperature. The vertical temperature structure, though, is quite different.

The initialization process of cloud liquid water from IFS HRES into WRF seems to work satisfyingly in the SCM simulation. The model produces Sc clouds at almost the right altitudes, as they are captured by the IFS, and the very low clouds at the first model levels do not form. The skin temperature develops in a more reasonable manner, with no major difference between the three methods.

Next, we test in a 3D simulation (90 vertical levels) with initialization in the whole domain using method B (Fig. 7). Here, also the cloud ice from IFS HRES is used, just to transfer as much cloud water and cloud ice as possible between the models. Figure 7a shows the cloud liquid water, potential temperature (red lines) and liquid potential temperature (blue lines). In a well-mixed adiabatic nonprecipitating cloud, the latter should be constant with height, while potential temperature should slightly increase with increasing height due to release of latent heat due to condensation. The simulated cloud clearly changes the vertical structure of the temperature profile, due to radiative cooling at cloud top, which creates convection forced by cooling at the top of the cloud.

The downwelling longwave radiation is shown for observations, SCM and 3D model results in Fig. 7b. We clearly see that the downwelling longwave radiation in the reference cases of both 3D and SCM are far too low compared to observations (black line), while the radiation in the cloud initialized runs are almost identical to observations, around 250 W m^{-2}. At 1200 UTC, the observed clouds are almost dissipated (Fig. 4a), and the downwelling radiation values decreases (Fig. 7b). However, the cloud in the 3D model persists too long compared to observations with consequences for the near-surface air temperature forecast that is too warm in all simulations toward the end of the simulation (Fig. 7c). All initialized simulations are too warm near the surface, which points to other issues than the cloud initialization.

Figure 8 shows vertical soundings every 6 h from observations, IFS analysis and 3D WRF simulations with cloud initialization using method A, i.e., the temperature and dewpoint are not changed at 0000 UTC. At this initial time, there are only small discrepancies between WRF and IFS HRES due to horizontal and vertical interpolation. The deficit between the temperature and dewpoint temperature profiles is a measure of the RH in the airmass. Two things are striking comparing the models against observations. First, the models cannot resolve the temperature structure near the surface even though this is comparison of an analysis against observations. This is a known problem in initialization of strong surface inversions. Apparently, resolution is only one part of the problem, because the inversion is absent in the analysis from IFS HRES and the host model is about 5°C too warm. The low temperatures in the near-surface air are discarded in the 4D VAR quality control, where, for example, the 2 m temperature is not used (L. Magnusson 2019, personal communication). Second, RH in the Sc layers in the observations seems to be 100%, as expected. This differs quite a lot compared to the RH in the models. At 0600 UTC IFS HRES still has a dewpoint deficit, while WRF has formed a vertical layer with RH close to 100%, where the cloud is present (Fig. 9). The implied cloud depth in WRF (400 m) is deeper than the observations (200 m). Also, the discrepancy between the models and the

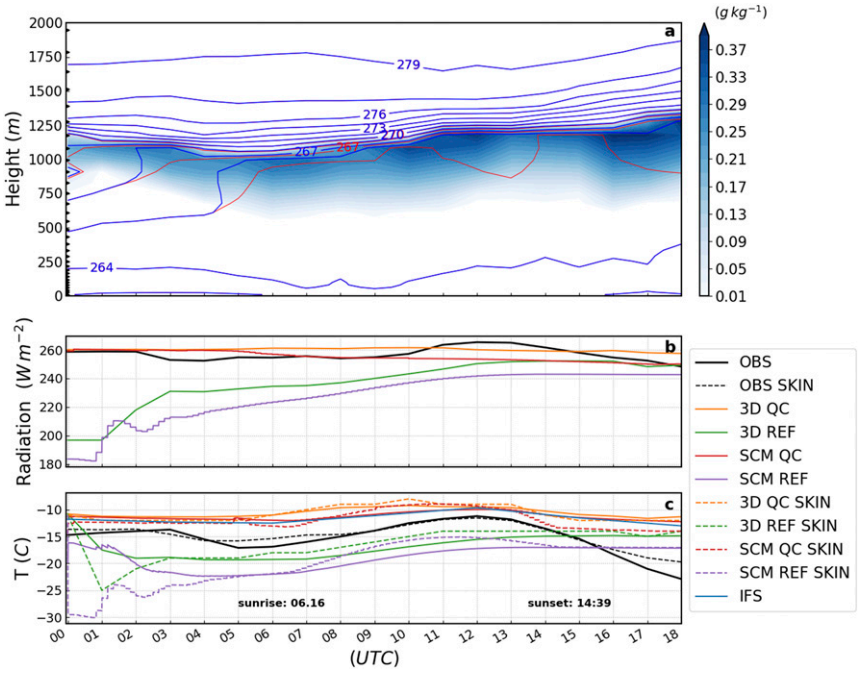

FIG. 7. 3D results for 18 h simulations started at 0000 UTC 18 Feb 2018. (a) Time–height cloud liquid water ($g\,kg^{-1}$; shaded), potential temperature (K; red), and liquid potential temperature (K; blue) cross section for 0000–1800 UTC 18 Feb 2018. Initialization with method B at levels with cloud liquid water values greater than $1 \times 10^{-2}\,g\,kg^{-1}$. (b) Downwelling longwave radiation at the surface ($W\,m^{-2}$) for observations (black), SCM reference (green), 3D reference (purple), SCM initialized clouds with method B (red), and 3D initialized clouds with method B (yellow). (c) 2 m temperature (°C; solid), and skin-temperature (°C; dashed) for the same simulations and with the same colors as in (b). Radiation observations are from the micrometeorological tower (67.362°N, 26.638°E) and temperature measurements are from the automatic weather station (67.367°N, 26.629°E).

observations at low levels has increased even more (Fig. 8b). Apparent in Fig. 9 is that IFS HRES produces cloud liquid water although relative humidities are well below saturation in the grid box, while WRF must have RH close to 100% to maintain the cloud. This displays the differences in the cloud parameterization schemes where IFS HRES and WRF have different critical relative humidities for cloud formation. Higher critical relative humidities leads to lower cloud fractions covering the grid box, where the cloud fraction usually is a function of the critical RH. Early, cloud ice is falling out, as snow, in WRF while IFS has mixed phase clouds and solid precipitation at all time steps. Cloud liquid water evolves similarly at the first three times, but at 1800 UTC cloud liquid water decreases in IFS HRES, while it is almost constant in WRF.

Cloud fraction profiles are very different in shape in the two models. In this configuration, WRF has a diagnostic cloud fraction (Xu and Randall 1996) that here gives values that are either 0 or 1 (Fig. 9c). This cloud fraction parameterization depends upon large-scale liquid water mixing ratio, RH and saturation water vapor mixing ratio. For small values of the liquid water mixing ratio, common in cold Arctic air, cloud fraction has a sharp transition from almost 0 to 1 for RH close to 100% (Lazarus and Krueger 1999). Although a critical RH (RHcrit) is not defined, it appears to have a value around 99%. In IFS HRES cloud fraction is a prognostic variable in a fully prognostic cloud scheme (Tiedtke 1993) that gives a dynamic range between 0 and 1 (Fig. 9g). It has a RHcrit of 0.8 that defines the width of the PDF of humidity in a clear-sky grid box, but just for the initial cloud formation. Once there is some cloud in the gridbox RHcrit is no longer used, as the PDF is then defined by the gridbox mean humidity and the prognostic cloud fraction (R. Forbes 2021, personal communication). Although an important operational forecast parameter, cloud fraction is of secondary concern, compared to cloud liquid water, when it comes to interaction with longwave radiation.

The WRF 3D performance is improved according to longwave radiation, skin temperature and 2 m temperature as well as in cloud cover (Fig. 10), when Sc clouds are initialized (Fig. 7). In Fig. 10b, the cloud fraction diagnostic is modified to provide nonzero values only when cloud liquid water content exceeds $10^{-3}\,g\,kg^{-1}$, which has little effect. In Fig. 10c, clouds are initialized with method B and the original scheme (Xu and Randall 1996) is used. This change affects the cloud-base values, but they are still too low compared to observations. In Fig. 10d method B is used with the modified cloud fraction

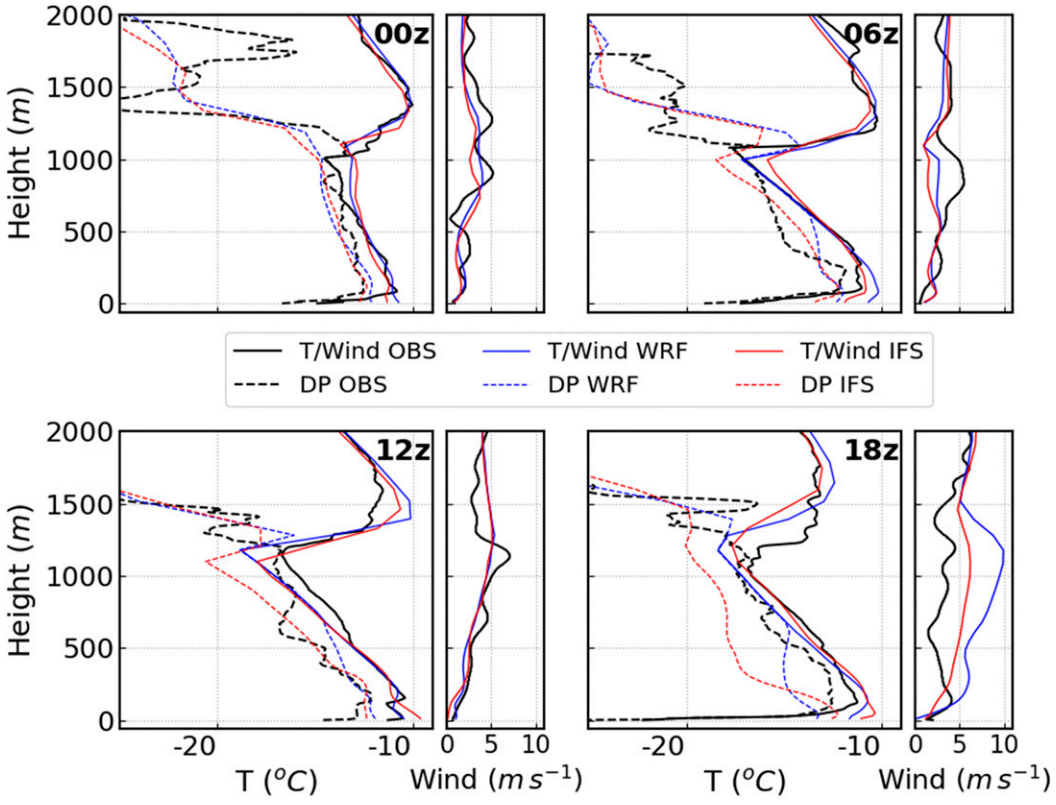

FIG. 8. 3D results for 18 h simulations started at 0000 UTC 18 Feb. Clouds initialized with method A. In large panels, vertical profiles of temperature (°C; solid), dewpoint (°C; dashed) and, in small panels, vertical profiles of wind speed (m s^{-1}) in IFS (red), WRF (blue), and observations (black) from Sodankylä sounding station (67.367°N, 26.629°E).

diagnostic. Now the cloud bases conform a lot better with observations at the site of Sodankylä (Fig. 4a). Other stations over land in the northern parts of Scandinavia show similar values as observed in Sodankylä (not shown). These weather situations, with cold air and temperature below −10°C in the whole cloud, provide perfect conditions for light snowfall to prevail intermittently for a long time (Fig. 4a). When the Sc clouds are initialized, light intermittent snowfall is formed in the model as in reality. Although small amounts of 0.2 mm rain per day falls in the model and 1.2 mm in reality (not shown), they are important for the moisture budget and also influence the thermodynamic structure through the latent heat redistribution and vertical stability as seen in marine Sc (Svensson et al. 2000). Maybe higher values in the reality are the reason for clouds dissolving faster in reality compared to the model. During 18 February 2018 impressive fall streaks are seen immediately when the Sc reforms between 1200 and 1400 UTC (Fig. 4a). Snowfall and subsidence dissipate the Sc clouds over again.

The inversion at cloud top is of comparable strength in WRF, IFS, and observations (Fig. 8). At 0600 UTC, it is almost identical in WRF and observations, but a bit weaker in IFS. At 1200 UTC, both IFS and WRF have inversions that are a bit too strong compared to observations, but at the right altitude. Figure 4a reveals that the observed Sc deck dissipates after about 0900 UTC and some thin sheet of Sc appear again around 1200 UTC, but at this time, WRF has a cloud layer from about 1150 m down to 700 m (Fig. 11a). After 1200 UTC, the cloud liquid water content in IFS HRES slowly decreases, while it is increasing in WRF. Observations (Fig. 4a) indicate Sc clouds at about 1000 m height during the evening, although it is not very well detected as there are backscatter values from low freezing fog that nearly saturate the signal. Supercooled fog is a rare condition on top of a snow surface at temperatures 25°C below freezing. The potential temperature structure in both models becomes more and more well mixed in, and below, the clouds as time passes (Figs. 11a,b). This is also seen in reality until 0600 UTC (Fig. 11c), but then, when the Sc slowly dissipates, the structure is stabilized again, because of less cloud-driven mixing.

The same vertical soundings as in Fig. 8 can be depicted in potential temperature instead (not shown). In the initial profile, the fine details in the observations are not resolved in the profile from IFS HRES analysis and there are discrepancies between IFS HRES and WRF due to the interpolation. An important observation is that the stratification in clouds in IFS is stable, while it is more well mixed in the observations. Observations of cloud liquid water are not available, so liquid

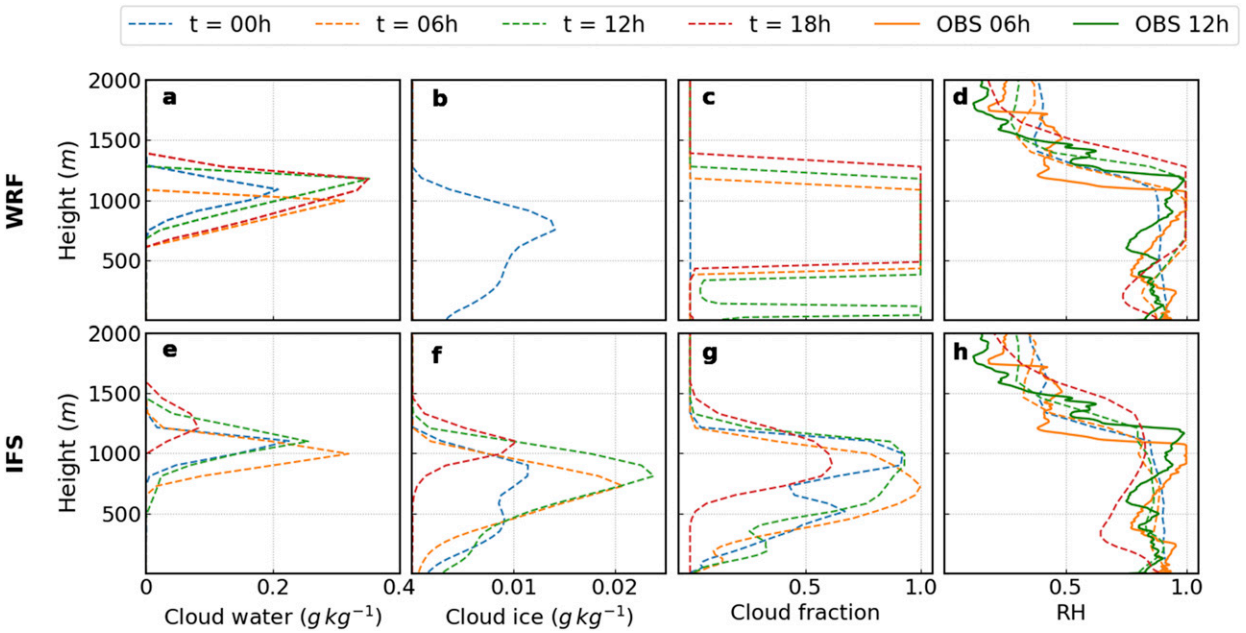

FIG. 9. 3D results for 18 h simulations started at 0000 UTC 18 Feb. Clouds initialized with method A at 0000 UTC (blue), 0000 + 0600 UTC (yellow), 0000 + 1200 UTC (green), and 0000 + 1800 UTC (red). Vertical profiles of (a) WRF cloud liquid water (g kg^{-1}), (b) WRF cloud ice (g kg^{-1}), (c) WRF cloud fraction, (d) WRF RH and observations RH, (e) IFS cloud liquid water, (f) IFS cloud ice, (g) IFS cloud fraction, and (h) IFS RH and observations RH. Observations are from Sodankylä sounding station (67.367°N, 26.629°E).

potential temperature cannot be calculated, but potential temperature would be increasing with height in an adiabatic cloud. At 0600 UTC potential temperature is constant both in and below clouds down to approximately 500 m in both WRF 3D and WRF SCM as well as in the observations, while the stratification in IFS is still too stable. As time passes, the SCM diverges more and more from the 3D run, which is to be expected due to neglecting advection and subsidence. At 1200 UTC, even the IFS HRES stratification is more well mixed, but at that time the observations are more stable again. At this time, a well-mixed layer is also seen close to the ground, in the models (Fig. 8), due to warming from the sun. Downwelling shortwave radiation at the surface is around 150 W m^{-2} at noon when the sky is clear. It is noticeable, however, that it is still stably stratified in the layer closest to the surface in the observations. This is not resolved in the models.

The case of 18 February 2018 that we have been discussing is a good example, when the 3D model performs quite well without any complex changes to the initial state. Just to

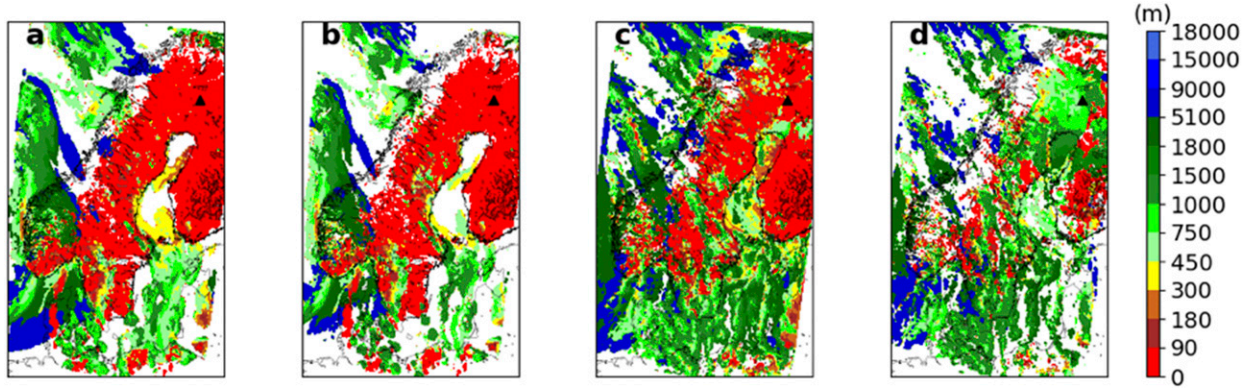

FIG. 10. 3D results for 3 h simulations started at 0000 UTC 18 Feb. (a) Cloud-base height (m) for reference case with Xu and Randall cloud fraction parameterization, (b) cloud parameterization changed to set cloud fraction equal to 1 if cloud liquid water exceeds 1×10^{-3} g kg^{-1}, (c) cloud liquid water and cloud ice initialized with method B together with Xu and Randall cloud fraction parameterization, and (d) cloud liquid water and cloud ice initialized with method B and cloud fraction parameterization that sets cloud fraction equal to 1 if cloud liquid water exceeds 1×10^{-3} g kg^{-1}.

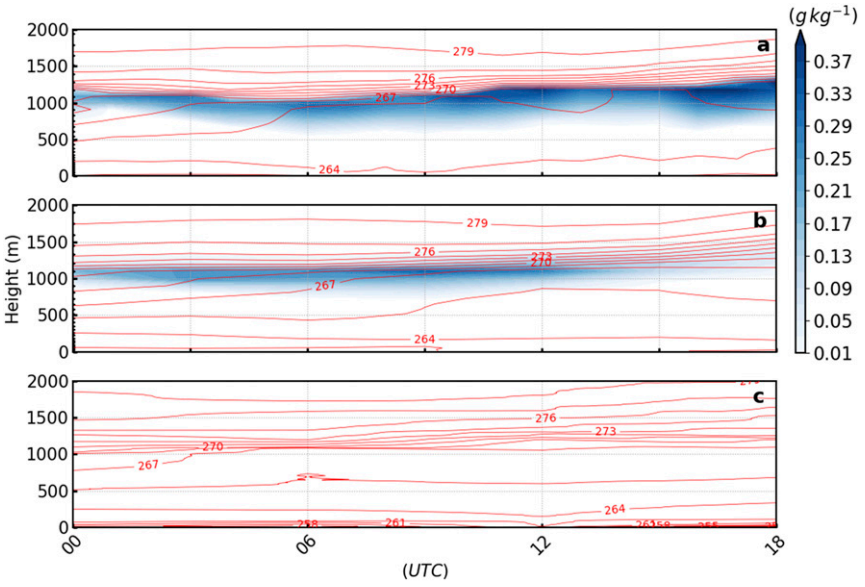

FIG. 11. Time–height cloud liquid water (g kg^{-1}) (shaded) and potential temperature (K) (red) for 18 h simulations started at 0000 UTC 18 Feb. Clouds initialized with method B for levels where cloud liquid water exceeds 1×10^{-2} g kg^{-1}. Time cross sections for (a) WRF potential temperature (K) and cloud liquid water, (b) IFS HRES potential temperature and cloud liquid water, and (c) potential temperature (K) constructed out of four soundings (0000, 0600, 1200, 1800 UTC) from Sodankylä sounding station (67.367°N, 26.629°E).

initialize cloud liquid water and cloud ice directly from IFS HRES with method A improves the model performance substantially and the modeled cloud bases compare well to the observations at Sodankylä (not shown). However, as seen in the SCM, the best performance of temperature, skin temperature and downwelling radiation is achieved with method B when RH is increased to 100% in the clouds. Examining the cloud bases over a larger area with and without initialization with method B clearly shows the improvement (Fig. 12a). The stratification in the IFS HRES is too stable in, and below, the low-level clouds. WRF 3D, on the other hand, keeps the clouds too long and the vertical extent of the clouds are too deep, i.e., the cloud bases are getting too low. It can also be seen that, northeast of the Sc clouds, patches of low clouds still form as Sc is dissipating and are advected toward the southwest (Fig. 10d). However, the observations at Sodankylä show low clouds in the evening (Fig. 4a). In any case, the modeled clouds are too widespread compared to the satellite imagery.

Apparently, IFS HRES parameterization schemes form cloud liquid water for RH values below 100% (Fig. 13a), which is not the case in WRF where RH close to 100% is needed (Fig. 13b). This explains why, for many situations, WRF cannot keep the cloud liquid water initialized in the WRF analysis. It only works in situations when the RH interpolated from IFS HRES is quite close to 100%, so that the cloud liquid water initialized does not evaporate completely.

Inspired by the improved results for the situation on the 18 February, we test methods A–C on a few more dates when

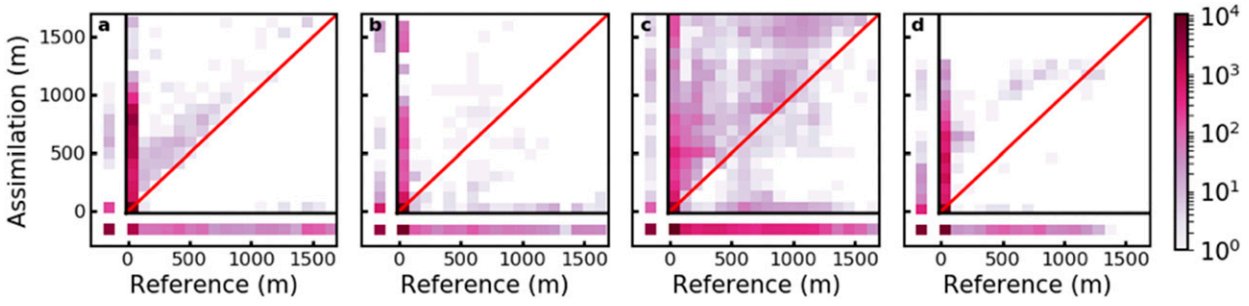

FIG. 12. Two-dimensional histograms of cloud-base height (m) for four 6 h reference simulations started at 0000 UTC 18 Feb 2018 and four 6 h simulations initialized with method B at vertical levels with cloud liquid water values $> 1 \times 10^{-2}$ g kg^{-1}: (a) 18 Feb, (b) 20 Feb, (c) 26 Feb, and (d) 27 Feb 2018. Grid points north and east of red lines in Fig. 1 are used. Hits at negative values at the two axes are when no clouds are modeled, which means clear skies.

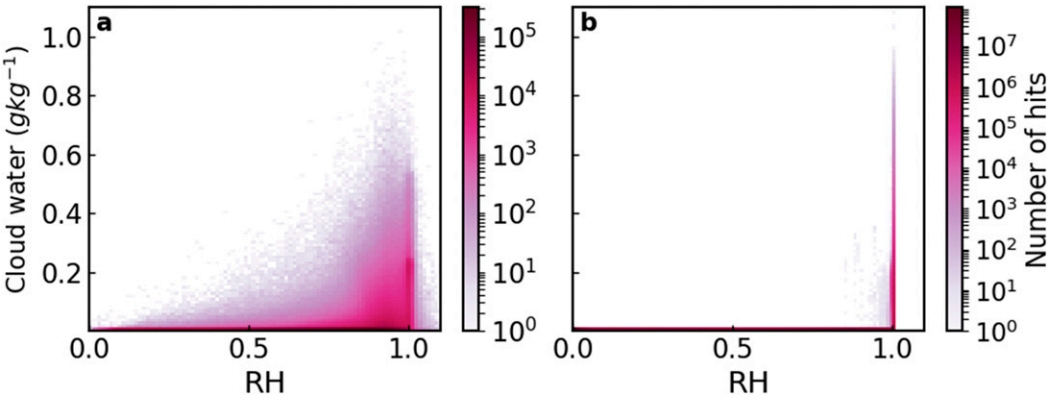

FIG. 13. Two-dimensional histograms for 3D 24 h simulations for cloud liquid water (g kg^{-1}) and RH started at 0000 UTC 18 Feb. (a) Cloud climatology for ECMWF every 3 h output file (analysis 0000 UTC and forecast steps) summed up and (b) cloud climatology for WRF reference simulation every 1 h output file (analysis 0000 UTC and forecast steps) summed up.

clouds were observed at Sodankylä. It turns out that for some of the dates, the 20, 26, and 27 February for example, there are no clouds in IFS HRES in the most northern parts of Sweden and Finland, including the Sodankylä location. Thus, no improvement is seen at Sodankylä. However, comparing over a larger area, it is clear that the cloud forecast is improved for these dates as the unrealistically low cloud bases are mostly removed (Fig. 12).

When cloud liquid water is missing completely in the host analysis from the IFS, it is not as straightforward to improve the analysis in the regional model and thereby the forecast quality. This particular forecast problem, concerning cloud free analysis but cloudy observations, is also highlighted in (Bannister et al. 2020). There are also cases when the host model has clouds but at the wrong altitude and/or wrong phase. The forecast quality is also hampered when there are clouds at wrong altitudes advected into the regional domain, which is the case on 26 February. An alternative approach to use in situations when there are no bulk liquid water or ice to transfer from the host model, although they exist in reality, is to use information from soundings. This approach is tested for the situation on 27 February.

2) CASE STUDY 2: 27 FEBRUARY 2018

The satellite picture on 27 February shows a low cloud deck over the area of interest (Fig. 14), which is confirmed in the observations at Sodankylä where a thin (about 200–300 m thick) cloud with base at 1100 m and top around 1300 m is observed between 0000 and 1000 UTC (Fig. 4b). The reference WRF forecast (Fig. 5b) shows the typical behavior with widespread fog. IFS HRES does not capture the observed Sc clouds in the analysis and there is no cloud liquid water nor cloud ice to transfer to WRF at the initial time. Instead we use information from the sounding at 0000 UTC 27 February 2018, utilizing the fact that in an adiabatically formed cloud, where 100% condensation is taking place, liquid potential temperature is constant with height. The initial profile is only modified in the cloud layer.

To investigate how WRF responds to this new way of initializing the clouds, we used the SCM for the site of Sodankylä. The SCM was initialized with the initial profile from the 3D analysis with the additional adiabatic cloud liquid water based on the observations at 0000 UTC and a simulation time of 15 h. Water vapor mixing ratio was increased to saturation water vapor mixing ratio, to better support the clouds (method D). Clouds may not be adiabatic so we utilized the observed magnitude of the downwelling longwave radiation and the surface temperature to find the consistent integrated liquid water content. By decreasing cloud liquid water step-by-step the downwelling radiation decreases, and at about 25% of the adiabatic cloud liquid water content, it was near the observation value, which also made the surface temperature coincide with observations (Fig. 15). For this case, additional simulations examining the impact of the PBL scheme were performed.

As the SCM is not forced with subsidence and advection, caution is necessary when examining the results in comparison with the observations at later times. Large-scale processes of subsidence and advection can never be assumed to be zero. In terms of ground-based site measurements, they cannot be directly observed either. The observed cloud is slowly sinking as a result of the large-scale subsidence (Fig. 4b). Despite the presence of Sc clouds, the temperature is rising even in the SCM from about 0600 UTC, when the skin temperature becomes higher than the 2 m temperature and a shallow, convective layer near the surface is developing (Figs. 15a,e). As time goes by, the stratification below clouds is slowly increasing in reality (not shown). This is not captured by any of the schemes.

To improve the low-level vertical temperature gradient, i.e., the sharp surface inversion, at the initialization time, simulations using the actual temperature profile from the radiosonde launch were performed (Fig. 16). The observed temperature profile was used at all model levels. The striking difference from Fig. 15, in the lower part of the PBL, is that the sharp initialized surface inversion at 0000 UTC is almost unaffected

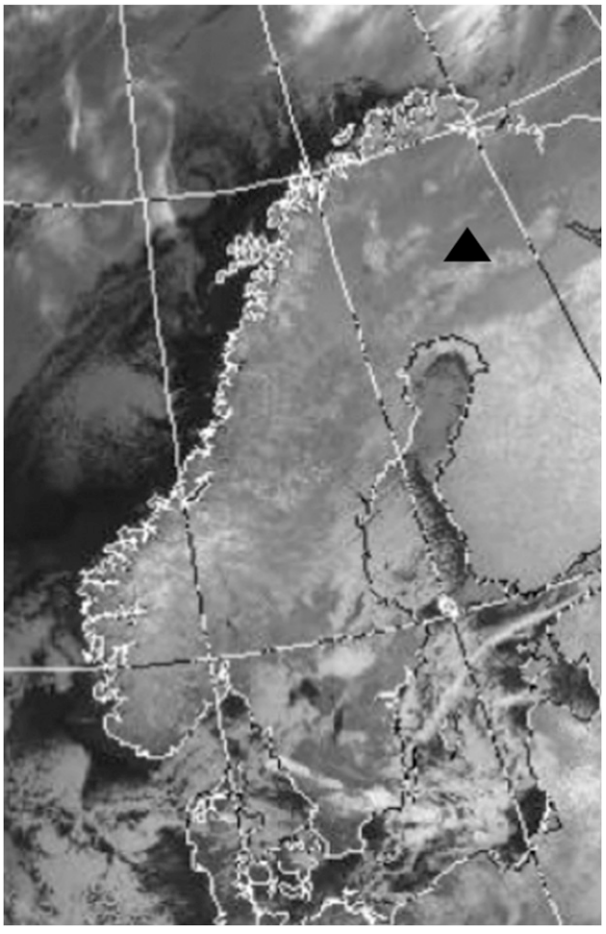

FIG. 14. Satellite IR image at 0332 UTC 27 Feb 2018 from the Advanced Very High Resolution Radiometer (AVHRR) channel 5 (10.5–12.5 μm) showing extensive areas of Sc clouds over the northern parts of Scandinavia. Clouds are broken and the colder surface (light gray) is seen at some spots (cf. with southern parts of Finland where sky is clear). Sodankylä is marked with a black triangle. Image is courtesy of NERC Satellite Receiving Station, Dundee University, Scotland, 2020 (http://www.sat.dundee.ac.uk/).

in the model at 0600 UTC (not shown), diverging from the observed profile. This is probably because the mixing in the lowest layers is almost zero in the SCM. In Fig. 15 the observed profile and the forecasted profile almost coincide at 0600 UTC, but it is a coincidence because they diverged at initialization time, when the sharp surface inversion existed in the observation, but not in the analysis.

Generalizing this method, initialization of clouds where they appear in the sounding at Sodankylä, to the 3D model, two simulations were performed. In both, it was assumed that the Sc cloud deck observed at Sodankylä was present over land everywhere over the northern parts of the domain, supported by the satellite picture (Fig. 14) and other observations (not shown). The benefits from this additional information in the initial fields clearly show impact (Fig. 17a) with a cloud layer that corresponds to observations (Fig. 4b) and a vertical temperature structure that is more similar to the observations (Fig. 17d). IFS (Fig. 17c) shows a different temperature structure as there is no cloud. However, because the too stable profile is initialized from the host model, the stratification in WRF is also too stable throughout the simulation. The surface inversion is too deep and not as sharp as in observations, especially around noon. This makes the convective part of the day at low levels, apparent in IFS and observations, much too shallow. Sc clouds dissipate 1–2 h earlier than in observations and very low clouds form, but just temporarily, in the middle of the day. In the late afternoon, the surface inversion is growing too fast in WRF and very low cloud forms.

The second simulation was performed using a revised initial profile with a surface inversion. This surface inversion is represented by the lowest 350 m of the Sodankylä sounding introduced in a terrain-following manner over the same area where the cloud layer is initialized. Further improvements are achieved by this as seen in Fig. 17. The lower part of the boundary layer (Fig. 17b) coincides better with observations (Fig. 17d) and even the stratification in and below clouds is weaker. This improvement is still apparent at the end of the model run. The surface inversion grows slower and low cloud forms even later than in the 3D-initialized simulation (Fig. 17a).

Finally, to show how cloud bases are affected by Sc initialization and type of cloud parameterization chosen, consider four additional, different 3D simulations started at 0000 UTC 27 February. Figure 18 shows the cloud base at 0600 UTC (top row) and 1500 UTC (bottom row) for the reference run (Figs. 18a,e, no cloud initialization), one changed cloud fraction diagnostic (Figs. 18b,f) and two cloud initialized runs. It is apparent that the initialization of the Sc clouds does increase the cloud-base height to be more consistent with observations, although the observed cloud deck is starting to break up (not shown). The model cloud at Sodankylä dissipates 1–2 h earlier than observed (not shown). When Sc clouds dissipate and are advected toward the southwest, very low clouds still form in the northeastern parts of the domain, but these amounts are reduced when the surface inversion is introduced (cf. Figs. 18c,d) and this is the case even at 1500 UTC (cf. Figs. 18g,h). Apparently, the initialization of the vertical temperature structure from Sodankylä sounding still improves the forecast after 15 h, which was also seen in Fig. 17. Later in the evening these improvements more or less disappear. Time–height cross sections shows that the stable layer near the ground still grows too fast compared to observations (not shown). The downwelling longwave radiation, under clear skies, is observed to be about 25 W m^{-2} larger in reality compared to the model (not shown). More investigations are needed to reveal the cause of this.

6. Discussion and conclusions

Since 2007 the Swedish Armed Forces (SAF) configuration of WRF 3.9.1.1 has had severe problems to represent low clouds over snow-covered areas. In a series of experiments, with both the full 3D model and a SCM version, we diagnose the root of the problem and suggest possible solutions. During the experiments results were continuously compared to

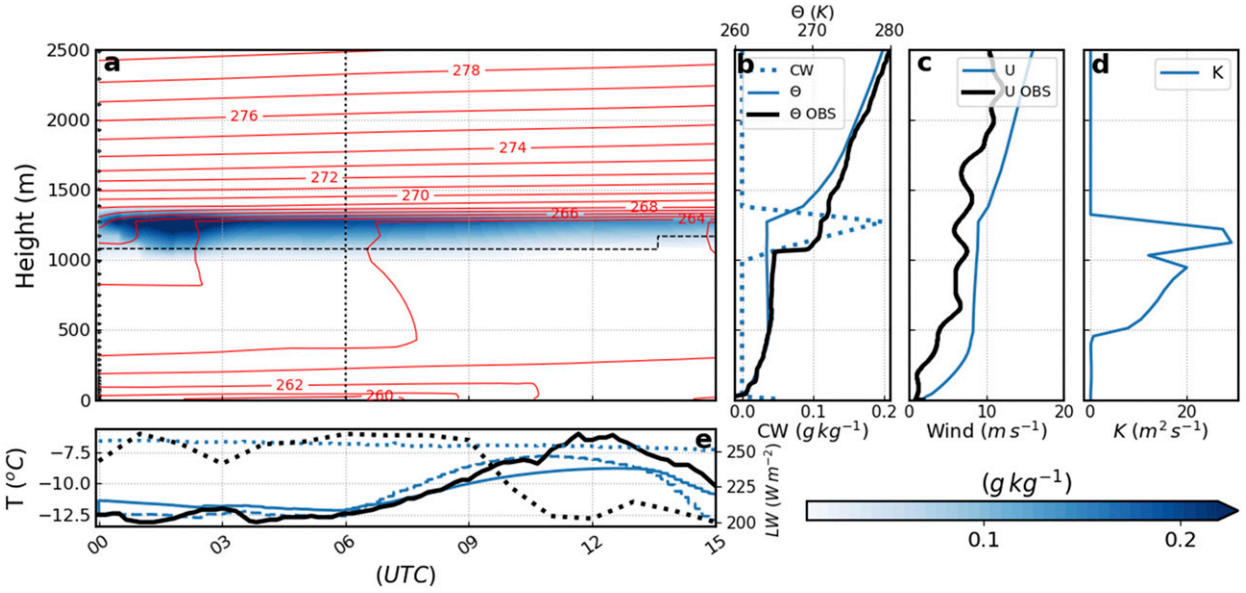

FIG. 15. SCM results for a 15 h simulation started at 0000 UTC 27 Feb with YSU and cloud liquid water (25% of adiabatic cloud amount) initialized from Sodankylä sounding and water vapor mixing ratio increased to saturation water vapor mixing ratio at levels where cloud liquid water is initialized (method D). (a) Potential temperature (K) (red) and cloud liquid water (g kg^{-1}; shaded). The vertical dashed line is time of the vertical profiles, and the horizontal black dashed line is the cloud base. (b) Vertical profiles of the potential temperature (K) from observations (black solid) and WRF (blue solid) and the cloud liquid water (blue, dotted). (c) Vertical profiles of wind (m s^{-1}) from observations (black solid) and WRF (blue solid). (d) Vertical profile of eddy diffusivity for heat and momentum (m^2 s^{-1}; blue solid). (e) Downwelling longwave radiation (W m^{-2}) from observations (black dotted) and WRF (blue dotted), 2 m temperature (°C) from observations (black solid) WRF (blue solid) and skin temperature (°C; blue dashed).

observations from the site of Sodankylä in the most northern parts of Finland. Although WRF is highly modular with multiple physics packages to choose from, the purpose has been to understand processes responsible for this deficiency, rather than testing different parameterizations.

Our experiments show that the problems arise in the initialization of the model. When the SAF WRF forecast begins, it is initialized with specific humidity, winds, temperature and skin temperature from IFS HRES, but no cloud information is passed from the host model. When low clouds are present in

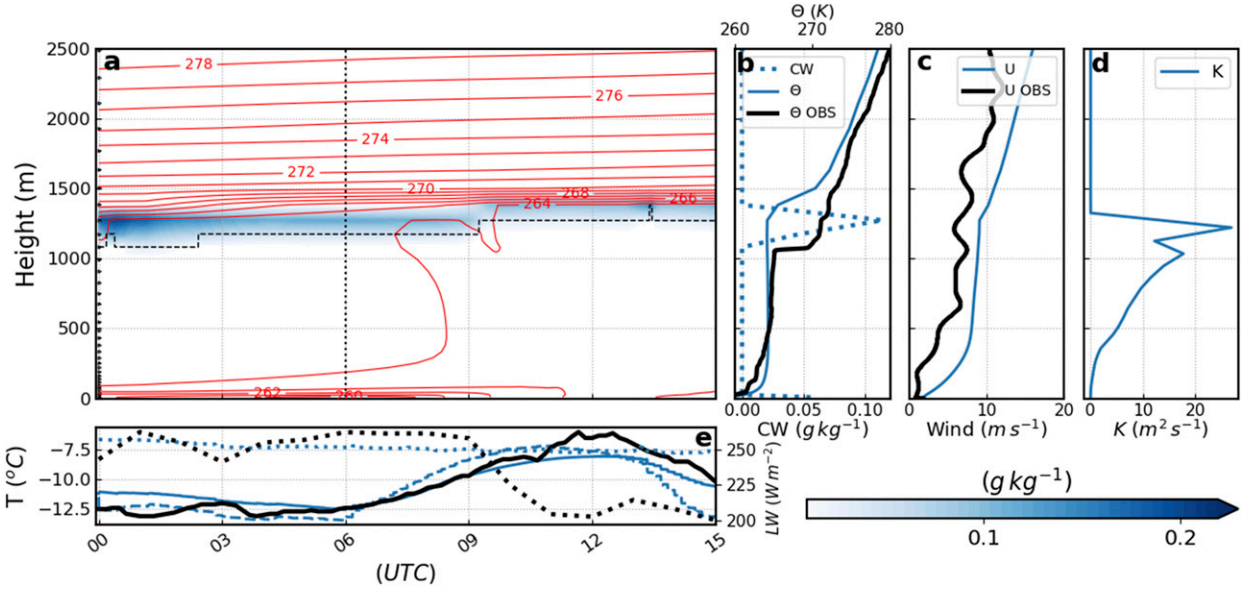

FIG. 16. As in Fig. 15, but initialized with the temperature profile from Sodankylä sounding 0000 UTC 27 Feb 2018.

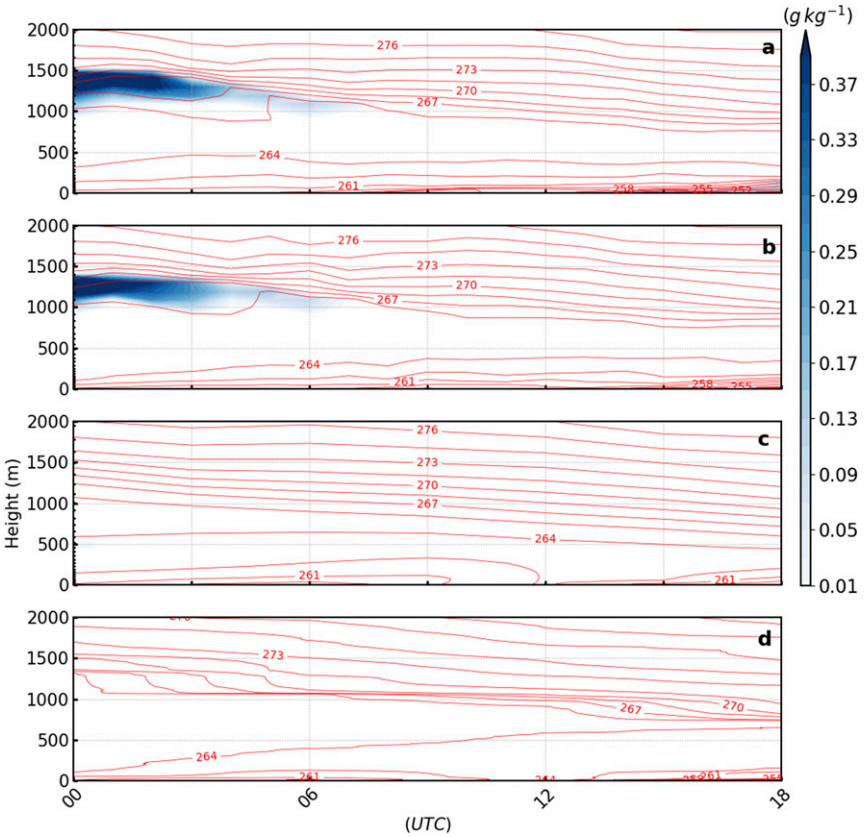

FIG. 17. Height–time cloud liquid water (g kg^{-1}; shaded) and potential temperature (K; red) for 18 h simulations. Clouds initialized north and east of the red lines in Fig. 1, at levels coinciding with Sodankylä sounding and water vapor mixing ratio increased to saturation water vapor mixing ratio at levels where cloud liquid water is initialized (method D). Time cross sections for (a) WRF 18 h simulation started at 0000 UTC 27 Feb (with YSU) potential temperature and cloud liquid water, (b) WRF 18 h simulation started at 0000 UTC 27 Feb potential temperature and cloud liquid water and lowest 350 m changed to Sodankylä sounding temperature profile, (c) IFS HRES potential temperature and cloud liquid water, and (d) potential temperature constructed out of four soundings (0000, 0600, 1200, 1800 UTC) from Sodankylä sounding station (67.367°N, 26.629°E).

reality, they increase the downwelling longwave radiation to the surface. This energy source at the surface is especially important in a stably stratified environment with sharp surface inversions as it affects the energy budget at the surface, which, in turn, sets the skin temperature and temperature in the lowest layer of the atmosphere. When no cloud information is available at the initial time in WRF, this energy is lacking during the first hours when WRF has to spin up its own clouds from the initialized humidity, a slow process in winter at high latitudes. With less downwelling longwave radiation, the deficit of energy at the surface leads to a rapid, unphysical drop in the skin temperature. Drops of 20°C in 20 s (one time step) have been noted. This leads to saturation, and clouds form at the first model level before Sc clouds have formed at higher altitudes. When this happens, the cloud top cools due to outgoing longwave radiation, more cloud liquid water forms, which in turn leads to increased outgoing longwave radiation, and so on. More and more cloud liquid water forms and the cloud slowly spreads to model levels at higher altitudes. Due to lack of incoming solar radiation at these times of the year, and the specific properties of the snow surface, these clouds can be persistent for a long time. The identified problem is typical for winter conditions in stably stratified conditions. In summer, the boundary layer is remixed every day as the energy available at the surface increases during the day and the model gets a ''new chance'' to perform better as it typically does in unstable conditions. Thus, biases that may develop due to deficiencies in the mixing and or radiation from clouds are forgotten when we have a more pronounced diurnal cycle. Our experiments have shown that these clouds, in WRF, consist of cloud liquid water amounts that are at least one order of magnitude greater than the cloud ice content. An unphysical regime develops as supercooled liquid water on top of a snow surface should not be persistent, unless humidity is advected continuously. In the central parts of anticyclones intermittently covering these parts of Earth in wintertime, substantial humidity advection is not

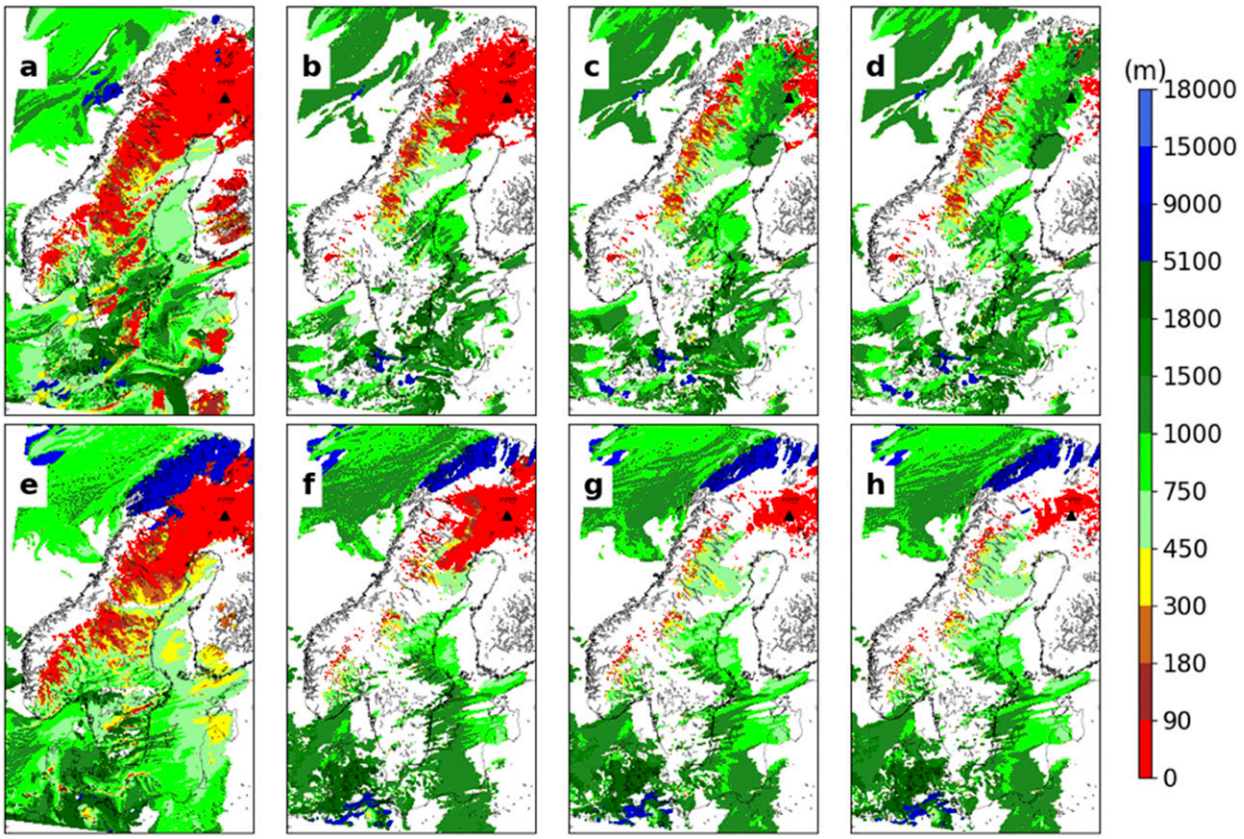

FIG. 18. 3D results for four simulations of cloud-base height (m) started at 0000 UTC 27 Feb. (a)–(d) A 6 h forecast valid at 0600 UTC 27 Feb 2018. (a) Reference simulation. (b) Cloud fraction parameterization changed from Xu and Randall to set cloud fraction equal to 1 if cloud liquid water exceeds 1×10^{-3} g kg^{-1}. (c) Initialized cloud liquid water, north and east of the red lines in Fig. 1, at levels coinciding with the sounding at Sodankylä at 0000 UTC 27 Feb 2018 and water vapor mixing ratio increased to saturation water vapor mixing ratio at levels where cloud liquid water is initialized (method D). (d) As in (c), but with temperature profile below 350 m AGL changed at every grid point to the lowest 350 m in the sounding from Sodankylä at 0000 UTC 27 Feb 2018. (e)–(h) As in (a)–(d), but for a 15 h forecast valid at 1500 UTC 27 Feb 2018.

common. From this point of view the persistence of these very low-level clouds is peculiar and further investigation is needed to understand how the model maintains them.

By interpolating bulk liquid water and bulk ice water content, respectively, from IFS HRES to WRF, we transferred these, as two different parts, to the initial profile in WRF (method A). Nevertheless, our experiments showed that WRF mostly was unable to keep these more than a few time steps. This is explained by the difference in thermodynamic environment that support clouds in IFS HRES and WRF. Cloud liquid water and cloud ice form and are sustained at a much broader spectrum of RH in IFS HRES while WRF needs nearly 100% RH for clouds to exist. Only in the few cases when IFS HRES had a RH of 100% in clouds, this method of WRF initialization was successful. By increasing RH in the WRF initial state at every vertical level where a certain amount of cloud liquid water was present after the interpolation (methods B and C), the ability to sustain clouds during the first time steps increased in SCM simulations. This was accomplished by either lowering the temperature (method B), or increasing the mixing ratio to reach the saturation point (method C). When the temperature was changed, static instability was introduced, that quickly remixed in the forthcoming time steps and did not cause any problems.

Further simulations with the SCM revealed that when the temperature was decreased (method B), cloud liquid water formed in amounts that was beneficial for a realistic development of the skin temperature. method B was then tested in the 3D model with much improved results. The amount of manipulation needed depends on the RH that is interpolated from IFS HRES to WRF. Method B works well in areas where Sc clouds are present in the IFS HRES analysis, but fails when they are not, or when clouds are present at wrong altitudes.

Further experimentation on how to initialize clouds was done in the SCM for the case of 27 February 2018, when clouds were present in reality but not in the IFS run. To estimate the cloud liquid water content to be added, we used the fact that the liquid potential temperature is constant in a well-mixed adiabatic Sc cloud (method D), which provides a theoretical upper bound of the cloud liquid water content (Stull 1988).

In our idealized SCM runs, only a small fraction of the theoretical value was needed to reach results that correspond to observations. A value of 25% of the adiabatic cloud liquid water content gave best agreement with observations. A larger cloud liquid water content led to too-high values of the downwelling longwave radiation, which led to higher skin temperatures. When clouds with small liquid water content were initialized in this way they remained in a well-mixed layer. However, in reality the clouds and the vertical mixing is influenced by large-scale forcing, such as subsidence and advection, which is not applied in the SCM experiments and thus leads to a different state than what was observed. Static stability in, and below, the clouds is important for the evolution. SCM runs showed that it took about 6 h to get the PBL mixed in the same way that was seen in the observed vertical soundings. Stratification in clouds in IFS HRES is greater than in WRF and in reality. If IFS HRES does not have any clouds at the WRF initialization time, the problem of too strong stratification in the initial profile is even more serious. When we initialized the SCM with the observed sounding from Sodankylä instead of the IFS profiles, the vertical structure was well mixed from the very beginning with a deep well-mixed layer and a shallow more stable surface inversion. Observations, though, are quickly influenced by large-scale subsidence and advection, making direct comparisons with the SCM difficult.

To maintain the cloud in the 3D model, initialization with the total adiabatic cloud liquid water content was needed. The Sc deck, present over northern part of Scandinavia, was quite homogeneous and was thus initialized similarly over this region. This substantially improved the forecast for the whole 24 h simulation. When Sc dissipated, very low clouds still formed at the first model level in the area of Sodankylä, but to a lesser extent than before. After correcting the lowest 350 m of the initial profile to contain the observed inversion at Sodankylä, even fewer very low clouds formed when Sc clouds dissipated, strengthening the importance of the vertical structure of temperature and humidity in the initial fields. Later in the simulation very low clouds still form even in areas where Sc clouds were initialized. Under clear skies both in the model and in reality, the downwelling longwave radiation at the surface in WRF is underestimated. If this is a consequence of the too sharp stratification at the surface or if the stratification is caused by the underestimated downwelling longwave radiation is difficult to say. The generation of very low clouds can also arise from deficiencies in the interaction between the land surface and the lowest part of the atmosphere. More investigations are needed to reveal the cause of this.

Sc clouds have a huge impact on the surface energy budget, and must be properly initialized when present in order to achieve reasonable forecasts. When Sc clouds are initialized in a correct way, our experiments also show that a correct initial temperature profile has more impact on the quality of the forecast than the parameterization scheme chosen.

This work has raised questions that should be considered in future studies. The optimum method for consistently modifying the thermodynamic profiles to support cloud liquid and ice is still an open question. One possibility is to modify temperature and humidity so that virtual potential temperature is conserved while achieving saturation. When cloud is present in observations but not in the host model, a SCM could be run, initialized with an observed sounding, to provide additional forecast guidance for a local area. The unphysical rapid decrease of snow surface temperature when cloud is not present suggests a flaw in the representation of snow properties, which should be explored. Finally, the persistence of fog over the snow surface suggests examination of the microphysics scheme.

Acknowledgments. MH acknowledges his employer, the Swedish Armed Forces (SAF), for the opportunity to conduct these full-time studies at MISU, during two years. The authors are also grateful for the ability to use SAFs computational resources at National Supercomputer Centre (NSC) basically intended for operational forecasting. Thanks to the WRF development team for support, and Rigel Kivi, Markku Kangas, Ewan O'Connor, and Roberta Pirazzini at FMI for help with observational data from Sodankylä. Thanks also to Victoria Sinclair, FMI, for valuable inputs in connection to my licentiate defense. Finally, thanks to Andreas Grantinger and Jacob Svensson, both in SAF, for help with issues regarding the WRF Model. WA is grateful to IMI for supporting his visit to Stockholm. WA was supported by NOAA Chemical Sciences Laboratory. Gunilla Svensson was supported by the EU H2020 Applicate Project (GA727862).

Data availability statement. Data from this project are stored at https://bolin.su.se/data/contributions/?d=5210&p=MjAyMC0xMC0yMCAwOToxNDozMi4xNjMxNSsgNTM3Nzg3MDM.

REFERENCES

Angevine, W. M., J. Olson, J. Kenyon, W. I. Gustafson, S. Endo, K. Suselj, and D. D. Turner, 2018: Shallow cumulus in WRF parameterizations evaluated against LASSO large-eddy simulations. *Mon. Wea. Rev.*, **146**, 4303–4322, https://doi.org/10.1175/MWR-D-18-0115.1.

Arduini, G., G. Balsamo, E. Dutra, J. J. Day, I. Sandu, S. Boussetta, and T. Haiden, 2019: Impact of a multi-layer snow scheme on near-surface weather forecasts. *J. Adv. Model. Earth Syst.*, **11**, 4687–4710, https://doi.org/10.1029/2019MS001725.

Balsamo, G., P. Viterbo, A. Beijaars, B. van den Hurk, M. Hirschi, A. K. Betts, and K. Scipal, 2009: A revised hydrology for the ECMWF model: Verification from field site to terrestrial water storage and impact in the integrated forecast system. *J. Hydrometeor.*, **10**, 623–643, https://doi.org/10.1175/2008JHM1068.1.

Bannister, R. N., H. G. Chipilski, and O. Martinez-Alvarado, 2020: Techniques and challenges in the assimilation of atmospheric water observations for numerical weather prediction towards convective scales. *Quart. J. Roy. Meteor. Soc.*, **146**, 1–48, https://doi.org/10.1002/qj.3652.

Bengtsson, L., and Coauthors, 2017: The HARMONIE-AROME model configuration in the ALADIN-HIRLAM NWP system. *Mon. Wea. Rev.*, **145**, 1919–1935, https://doi.org/10.1175/MWR-D-16-0417.1.

Benjamin, S. G., and Coauthors, 2016: A North American hourly assimilation and model forecast cycle: The Rapid Refresh.

Mon. Wea. Rev., **144**, 1669–1694, https://doi.org/10.1175/MWR-D-15-0242.1.

Bosveld, F. C., and Coauthors, 2014: The third GABLS intercomparison case for evaluation studies of boundary-layer models. Part B: Results and process understanding. *Bound.-Layer Meteor.*, **152**, 157–187, https://doi.org/10.1007/s10546-014-9919-1.

Chen, F., and J. Dudhia, 2001: Coupling and advanced land surface-hydrology model with the Penn State–NCAR MM5 modeling system. Part I: Model implementation and sensitivity. *Mon. Wea. Rev.*, **129**, 569–585, https://doi.org/10.1175/1520-0493(2001)129<0569:CAALSH>2.0.CO;2.

Courtier, P., 1998: The ECMWF implementation of three-dimensional variational assimilation (3D-Var). I: Formulation. *Quart. J. Roy. Meteor. Soc.*, **124**, 1783–1807, https://doi.org/10.1002/qj.49712455002.

Dybbroe, A., K. G. Karlsson, and A. Thoss, 2005: NWCSAF AVHRR cloud detection and analysis using dynamic thresholds and radiative transfer modeling. Part I: Algorithm description. *J. Appl. Meteor.*, **44**, 39–54, https://doi.org/10.1175/JAM-2188.1.

Geer, A. J., and Coauthors, 2018: All-sky satellite data assimilation at operational weather forecasting centres. *Quart. J. Roy. Meteor. Soc.*, **144**, 1191–1217, https://doi.org/10.1002/qj.3202.

Hacker, J. P., and W. M. Angevine, 2013: Ensemble data assimilation to characterize surface-layer errors in numerical weather prediction models. *Mon. Wea. Rev.*, **141**, 1804–1821, https://doi.org/10.1175/MWR-D-12-00280.1.

Häggmark, L., K. I. Ivarsson, S. Gollvik, and P. O. Olofsson, 2000: Mesan, an operational mesoscale analysis system. *Tellus*, **52A**, 2–20, https://doi.org/10.3402/tellusa.v52i1.12250.

Han, M., S. A. Braun, T. Matsui, and C. R. Williams, 2013: Evaluation of cloud microphysics schemes in simulations of a winter storm using radar and radiometer measurements. *J. Geophys. Res.*, **118**, 1401–1419, https://doi.org/10.1002/jgrd.50115.

Holtslag, A. A. M., and Coauthors, 2013: Stable atmospheric boundary layers and diurnal cycles: Challenges for weather and climate models. *Bull. Amer. Meteor. Soc.*, **94**, 1691–1706, https://doi.org/10.1175/BAMS-D-11-00187.1.

——, G. Svensson, S. Basu, B. Beare, F. C. Bosveld, and J. Cuxart, 2012: Overview of the GEWEX Atmospheric Boundary Layer Study (GABLS). *Proc. Working Diurnal Cycles Stable Boundary Layer*, Shinfield, Reading, ECMWF, 11–23.

Hong, S. Y., 2010: A new stable boundary-layer mixing scheme and its impact on the simulated East Asian summer monsoon. *Quart. J. Roy. Meteor. Soc.*, **136**, 1481–1496, https://doi.org/10.1002/qj.665.

——, and H. L. Pan, 1996: Nonlocal boundary layer vertical diffusion in a medium-range forecast model. *Mon. Wea. Rev.*, **124**, 2322–2339, https://doi.org/10.1175/1520-0493(1996)124<2322:NBLVDI>2.0.CO;2.

——, Y. Noh, and J. Dudhia, 2006: A new vertical diffusion package with an explicit treatment of entrainment processes. *Mon. Wea. Rev.*, **134**, 2318–2341, https://doi.org/10.1175/MWR3199.1.

Hu, X. M., J. W. Nielsen-Gammon, and F. Zhang, 2010: Evaluation of three planetary boundary layer schemes in the WRF Model. *J. Appl. Meteor. Climatol.*, **49**, 1831–1844, https://doi.org/10.1175/2010JAMC2432.1.

Jiménez, P. A., J. Dudhia, J. F. González-Rouco, J. Navarro, J. P. Montávez, and E. García-Bustamante, 2011: A revised scheme for the WRF surface layer formulation. *Mon. Wea. Rev.*, **140**, 898–918, https://doi.org/10.1175/MWR-D-11-00056.1.

Jung, T., and Coauthors, 2016: Advancing polar prediction capabilities on daily to seasonal time scales. *Bull. Amer. Meteor. Soc.*, **97**, 1631–1647, https://doi.org/10.1175/BAMS-D-14-00246.1.

Kangas, M., L. Rontu, C. Fortelius, M. Aurela, and A. Poikonen, 2016: Weather model verification using Sodankylä mast measurements. *Geosci. Instrum. Methods Data Syst.*, **5**, 75–84, https://doi.org/10.5194/gi-5-75-2016.

Lazarus, S. M., and S. K. Krueger, 1999: An evaluation of the Xu-Randall cloud fraction parameterization using ASTEX data. *Ninth ARM Science Team Meeting Proc.*, San Antonio, TX, 1–9.

LeMone, M. A., and Coauthors, 2019: 100 years of progress in boundary layer meteorology. *A Century of Progress in Atmospheric and Related Sciences: Celebrating the American Meteorological Society Centennial, Meteor. Monogr.*, No. 59, 9.1–9.85, https://doi.org/10.1175/AMSMONOGRAPHS-D-18-0013.1.

Mlawer, E. J., S. J. Taubman, P. D. Brown, M. J. Iacono, and S. A. Clough, 1997: Radiative transfer for inhomogeneous atmospheres: RRTM, a validated correlated-k model for the longwave. *J. Geophys. Res.*, **102**, 16 663–16 682, https://doi.org/10.1029/97JD00237.

Nakanishi, M., and H. Niino, 2009: Development of an improved turbulence closure model for the atmospheric boundary layer. *J. Meteor. Soc. Japan*, **87**, 895–912, https://doi.org/10.2151/jmsj.87.895.

Owens, R. G., and T. D. Hewson, 2018: ECMWF Forecast User Guide. ECMWF, https://doi.org/10.21957/m1cs7h.

Poulos, G. S., and Coauthors, 2002: CASES-99 : A comprehensive investigation of the stable nocturnal boundary layer. *Bull. Amer. Meteor. Soc.*, **83**, 555–582, https://doi.org/10.1175/1520-0477(2002)083<0555:CACIOT>2.3.CO;2.

Price, J., A. Porson, and A. Lock, 2015: An observational case study of persistent fog and comparison with an ensemble forecast model. *Bound.-Layer Meteor.*, **155**, 301–327, https://doi.org/10.1007/s10546-014-9995-2.

Renshaw, R., and P. N. Francis, 2011: Variational assimilation of cloud fraction in the operational Met Office Unified Model. *Quart. J. Roy. Meteor. Soc.*, **137**, 1963–1974, https://doi.org/10.1002/qj.980.

Savijärvi, H., 2014: High-resolution simulations of the night-time stable boundary layer over snow. *Quart. J. Roy. Meteor. Soc.*, **140**, 1121–1128, https://doi.org/10.1002/qj.2187.

Schmetz, J., P. Pili, S. Tjemkes, D. Just, J. Kerkmann, S. Rota, and A. Ratier, 2002: An introduction to Meteosat Second Generation (MSG). *Bull. Amer. Meteor. Soc.*, **83**, 977–992, https://doi.org/10.1175/1520-0477(2002)083<0977:AITMSG>2.3.CO;2.

Skamarock, W. C., and Coauthors, 2008: A description of the Advanced Research WRF version 3. NCAR Tech Note NCAR/TN-475+STR, 113 pp., https://doi.org/10.5065/D68S4MVH.

Smirnova, T. G., J. M. Brown, S. G. Benjamin, and J. S. Kenyon, 2016: Modifications to the Rapid Update Cycle land surface model (RUC LSM) available in the Weather Research and Forecasting (WRF) Model. *Mon. Wea. Rev.*, **144**, 1851–1865, https://doi.org/10.1175/MWR-D-15-0198.1.

Sterk, H. A. M., G. J. Steeneveld, T. Vihma, P. S. Anderson, F. C. Bosveld, and A. A. M. Holtslag, 2015: Clear-sky stable boundary layers with low winds over snow-covered surfaces. Part 1: WRF model evaluation. *Quart. J. Roy. Meteor. Soc.*, **141**, 2165–2184, https://doi.org/10.1002/qj.2513.

Stull, R. B., 1988: *An Introduction to Boundary Layer Meteorology*. Kluwer Academic, 666 pp.

Sultana, R., K. L. Hsu, J. Li, and S. Sorooshian, 2014: Evaluating the Utah Energy Balance (UEB) snow model in the Noah land-surface model. *Hydrol. Earth Syst. Sci.*, **18**, 3553–3570, https://doi.org/10.5194/hess-18-3553-2014.

Sun, J., and Coauthors, 2015: Review of wave-turbulence interactions in the stable atmospheric boundary layer. *Rev. Geophys.*, **53**, 956–993, https://doi.org/10.1002/2015RG000487.

Svensson, G., M. Tjernström, and D. Koračin, 2000: The sensitivity of a stratocumulus transition: Model simulations of the ASTEX first Lagrangian. *Bound.-Layer Meteor.*, **95**, 57–90, https://doi.org/10.1023/A:1002434314651.

——, and Coauthors, 2011: Evaluation of the diurnal cycle in the atmospheric boundary layer over land as represented by a variety of single-column models: The second GABLS Experiment. *Bound.-Layer Meteor.*, **140**, 177–206, https://doi.org/10.1007/s10546-011-9611-7.

Tiedtke, M., 1993: Representation of clouds in large-scale models. *Mon. Wea. Rev.*, **121**, 3040–3061, https://doi.org/10.1175/1520-0493(1993)121<3040:ROCILS>2.0.CO;2.

Tjernström, M., G. Svensson, L. Magnusson, I. M. Brooks, J. Prytherch, J. Vüllers, and G. Young, 2021: Central Arctic weather forecasting: Confronting the ECMWF IFS with observations from the Arctic Ocean 2018 expedition. *Quart. J. Roy. Meteor. Soc.*, **147**, 1278–1299, https://doi.org/10.1002/qj.3971.

Undén, P., and Coauthors, 2002: High Resolution Limited Area Model, HIRLAM-5 Scientific Documentation. Swedish Meteorological and Hydrological Institute, 144 pp., http://hdl.handle.net/20.500.11765/6323.

van der Veen, S. H., 2013: Improving NWP model cloud forecasts using Meteosat Second-Generation imagery. *Mon. Wea. Rev.*, **141**, 1545–1557, https://doi.org/10.1175/MWR-D-12-00021.1.

Xu, K. M., and D. A. Randall, 1996: A semiempirical cloudiness parameterization for use in climate models. *J. Atmos. Sci.*, **53**, 3084–3102, https://doi.org/10.1175/1520-0469(1996)053<3084:ASCPFU>2.0.CO;2.

Yucel, I., W. J. Shuttleworth, R. T. Pinker, L. Lu, and S. Sorooshian, 2002: Impact of ingesting satellite-derived cloud cover into the regional atmospheric modeling system. *Mon. Wea. Rev.*, **130**, 610–628, https://doi.org/10.1175/1520-0493(2002)130<0610:IOISDC>2.0.CO;2.

Zhang, T., 2005: Influence of the seasonal snow cover on the ground thermal regime: An overview. *Rev. Geophys.*, **43**, RG4002, https://doi.org/10.1029/2004RG000157.